AER/AGS Open File Report 2022-02

Alberta Energy Regulator

Relative Landslide Susceptibility Model of the Alberta Plains and Shield Regions, Version 2: Technical Documentation

AGS
ALBERTA GEOLOGICAL SURVEY

AER/AGS Open File Report 2022-02

Relative Landslide Susceptibility Model of the Alberta Plains and Shield Regions, Version 2: Technical Documentation

S.M. Pawley[1], S. Chowdhury[1], G.M.D. Hartman[1], D.K. Chao[1] and S.V. Samsonov[2]

[1] Alberta Energy Regulator
Alberta Geological Survey
[2] Canada Centre for Mapping and Earth Observation

October 2022

ISBN 978-1-4601-5352-9

Pawley, S.M., Chowdhury, S., Hartman, G.M.D., Chao, D.K. and Samsonov, S.V. (2022): Relative landslide susceptibility model of the Alberta Plains and shield regions, version 2: technical documentation; Alberta Energy Regulator / Alberta Geological Survey, AER/AGS Open File Report 2022-02, 30 p.

Publications in this series have undergone only limited review and are released essentially as submitted by the author.

Author address:
S.V. Samsonov
Natural Resources Canada
Canada Centre for Mapping and Earth Observation
560 Rochester Street
Ottawa, ON K1S 4M2
Canada
Tel: 343.292.6096
Email: sergey.samsonov@canada.ca, samsonov@insar.ca

Published October 2022 by:
Alberta Energy Regulator
Alberta Geological Survey
4th Floor, Twin Atria Building
4999 – 98th Avenue
Edmonton, AB T6B 2X3
Canada

Tel: 780.638.4491
Email: AGS-Info@aer.ca
Website: www.ags.aer.ca

Contents

Tables

Figures

Acknowledgements

We thank Dan Utting for the critical review and edit of the original manuscript.

Abstract

In 2016, the Alberta Geological Survey published the landslide susceptibility model of the Alberta Plains and Canadian Shield regions using a machine learning prediction that ranked the similarity of geological, physiographic, and climate conditions relative to locations affected by landslides. This document describes an update to this model (version 2) that makes use of more defined topographic information derived from a digital elevation model (DEM), created from light detection and ranging (LiDAR) data, and incorporates new landslide locations, which were compiled from multiple data sources including high-resolution, multitemporal satellite imagery and satellite interferometric synthetic aperture radar (InSAR) data, used to monitor ground deformation. Version 2 of the landslide susceptibility model provides a more accurate prediction of where future landslides or landslide reactivations are likely to occur, because the model incorporates new information relating to the spatial distribution of historically active landslides. The Alberta Geological Survey has also published (a) a map portraying the information in the new model, (b) the digital raster data, and (c) a compilation of historical landslide locations.

1 Introduction

Landslides in the Alberta portion of the Western Canada Sedimentary Basin (WCSB; Figure 1) occur within specific topographic settings, narrow and contiguous zones along the margins of incised river valleys and more broadly around the flanks of many regional uplands. Landslides as natural processes have contributed to valley widening and upland denudation throughout the Holocene. However, from a human perspective, they are disruptive and economically costly (Porter et al., 2019) because they can damage infrastructure and can render land unsuitable for development unless mitigative measures are put in place.

Landslide susceptibility maps represent a widely used approach to identify landslide-prone terrain on a regional scale and to prioritize smaller areas for more detailed inspections. Landslide susceptibility provides an estimation of where landslides are likely to occur, formally defined as a spatial probability that is time independent (Parise, 2001) and is based on the spatial distribution of conditions that cause landslides (Reichenbach et al., 2018). These conditions can be determined from physical models or qualitative criteria, but most commonly landslide susceptibility models (LSMs) use a statistical relationship between the spatial distribution of past landslides and a suite of predisposing topographic, geological, and climatic factors. However, landslides are also influenced by time-dependent factors including short-term triggering events such as rainfall, as well as longer term climatic changes, neotectonics, and patterns of landscape evolution. Consequently, although LSMs strictly estimate only the spatial probability of terrain being affected by landslides, LSMs may incorporate temporal constraints by using landslide inventories that relate to specific events, for example, weather events, a specific 'historical' timeframe, or different dates as part of a multitemporal inventory (Reichenbach et al., 2018). These LSMs are generally considered to be superior to those based on the geomorphological record of past landslides alone because they test the assumption that future landslides will occur under the same conditions as past landslides.

In practice, most event-based or multitemporal LSMs are for mountainous regions where modelling relies upon historical landslide records or landslides mapped from multitemporal aerial or satellite imagery. These landslides are typically rapidly moving failures that have abrupt initiations and do not show prolonged periods of movement. However, in the WCSB, which is dominated by lowland to moderate-relief upland terrain, landslides include deep-seated earthslides, earthflows, or complexes thereof, which do not show a single initiation event, but rather are characterized by long periods of stationary or extremely limited creep-type movement, punctuated by shorter/intermittent periods of increased movement rates due to triggering factors. Furthermore, these landslides typically occur within broad swathes of pre-existing landslide debris and colluvial deposits, which include components that may have been formed under early Holocene periglacial or paraglacial conditions (Thomson and Morgenstern, 1977; Ruban, 1983). These circumstances are problematic for using a traditional geomorphologically based approach because (a) past landslide locations may not be representative of where future landslides are likely to occur, and (b) the approach does not evaluate the potential for reactivation or new failures developing within existing landslide terrain. This makes it unclear as to how the geomorphological record of landslides relates to the concept of 'present-day' susceptibility, which limits the practical use of the susceptibility maps. In the context of the WCSB and other similar regions, a geomorphologically based approach (e.g., version 1 of this model [Pawley at al., 2016]) would amount to considering all landslide terrain as equally susceptible, which is likely to lead to many false positives with respect to identifying locations where future landslides are likely to occur.

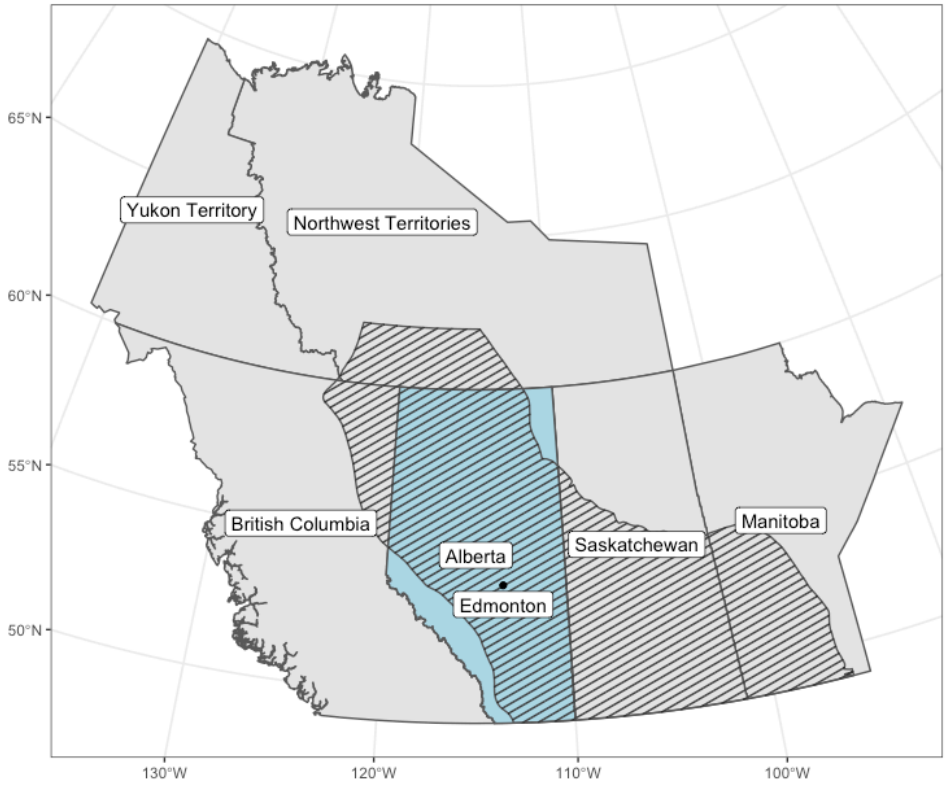

Figure 1. Western Canada Sedimentary Basin (WCSB; hatched area) and associated Canadian provinces and territories.

An alternative consideration of landslide susceptibility is that it is better described by estimating the probability that pre-existing landslide terrain will transition from a dormant or extremely slow-moving state, where the overall movement is small, to a state of activity where landslide movement velocities pose more substantial risks to infrastructure. One potential approach to capture this is to separate the prediction of the spatial distribution of landslides from the probability that these landslides will reactivate over a predefined time period. Conceptually, this approach is similar to that used by Dewitte et al. (2010), who estimated the potential for landslide reactivation along headscarps within previously mapped landslide bodies in west Belgium.

2 Landslide Susceptibility Model, Version 2

In 2016, the Alberta Geological Survey published the landslide susceptibility model of the Alberta portion of the WCSB, which is covered by the Alberta Plains, and the Canadian Shield in northeastern Alberta (Pawley et al., 2016). This model was based on a machine learning prediction that ranked the similarity of geological, physiographic, and climate conditions relative to locations affected by landslides. The predictions from this model represent a time-independent, spatial probability that a pixel (i.e., a defined area) may contain a landslide but did not evaluate the potential for landslide reactivation or new failures occurring within existing landslide terrain because information relating to the timing of landslide activity was not available at a provincial scale. However, in the WCSB, landslide reactivation and movement on existing landslides represents the main source of hazard (Porter et al., 2019). This model also relied upon terrain information from the relatively coarse-resolution Shuttle Radar Topography Mission (SRTM) digital elevation model (DEM), with a 90 m horizontal resolution.

Newly available terrain information derived from an almost provincially complete light detection and ranging (LiDAR) DEM, in addition to the ability to use provincially available, high-resolution,

multitemporal aerial and satellite imagery and ground deformation monitoring from satellite interferometric synthetic aperture radar (InSAR) data, provided new possibilities to update this previous work. New data compilation from published sources and new landslide detection from satellite data has provided the potential to evaluate landslide susceptibility both in terms of the spatial distribution of landslide terrain, and the probability that this terrain will reactivate. The updated version 2 landslide susceptibility model described in this document incorporates both components by using a nested susceptibility modelling approach, where an initial model is used to detect the areal footprint of landslide, and then a second model is used to estimate landslide susceptibility based on an inventory of landslides that show evidence of reactivation within a historical timeframe (i.e., during the past 50–100 years approximately). This approach has the advantage that the landslide susceptibility more closely estimates the locations where future slope failures are likely to occur, but the geomorphological footprint of all landslides, irrespective of their inferred activity status, is still portrayed in the map. This latter aspect is important because all landslides pose some potential hazard, irrespective of their activity state, especially if the balance of driving and resisting forces is altered (e.g., construction, drainage diversion, channel lateral movement or avulsion, deforestation, irrigation, etc.).

3 Input Data

3.1 Geology and Land Cover

Regional geological conditions represent important factors in landslide susceptibility because bedrock and surficial geology govern rock and sediment lithology and mechanical properties. Three sources of geological data were incorporated in this study: (1) bedrock geology, (2) surficial geology, and (3) soil/sediment thickness (Figure 2). Bedrock lithology was incorporated by reclassifying the varying lithological descriptions of bedrock formations in Alberta (Prior et al., 2013) into a unifying categorization of relative rock strength (Pawley et al., 2016). The composition of unconsolidated sediments at the surface was estimated from surficial mapping data (Fenton et al., 2013). Thirteen genetically defined classes were used to describe the general surface material characteristics. The thickness of the surficial sediments (Atkinson et al., 2020) was also used as a predictor because some highly landslide-prone areas have previously been associated with regions of high sediment thickness controlled by the distribution of buried paleochannel networks (Miller, 2000; Miller and Cruden, 2002; Morgan et al., 2012). Finally, land-cover data from Castilla et al. (2014) was included as an additional predictor because land-cover types, such as shrubland, grassland, or exposed land, may be indicative of landslide occurrences.

3.2 Distance-Related Features

Euclidean distance-based measurements to structural lineaments (Prior et al., 2013), stream channels, roads, and glaciotectonic ridges (Atkinson et al., 2014) were included as predictors (Figure 3) based on their potential to destabilize slopes. The distance to stream channels was calculated for streams that were extracted from the LiDAR DEM at 30 m resolution using several Strahler order thresholds (5, 6, 7 orders) to capture potential differences in stream power.

3.3 Precipitation

Precipitation-related predictors from the ClimateWNA gridded datasets (Wang et al., 2012) were included (Figure 4) to quantify the large precipitation differences that occur across Alberta. Precipitation differences strongly influence slope stability; for example, the Upper Cretaceous Horseshoe Canyon Formation, which comprises a succession of mudstone, sandstone, carbonaceous shale, and bentonite, is highly prone to landslides in the Edmonton region, but is more stable in southeastern Alberta where the climate is comparatively arid.

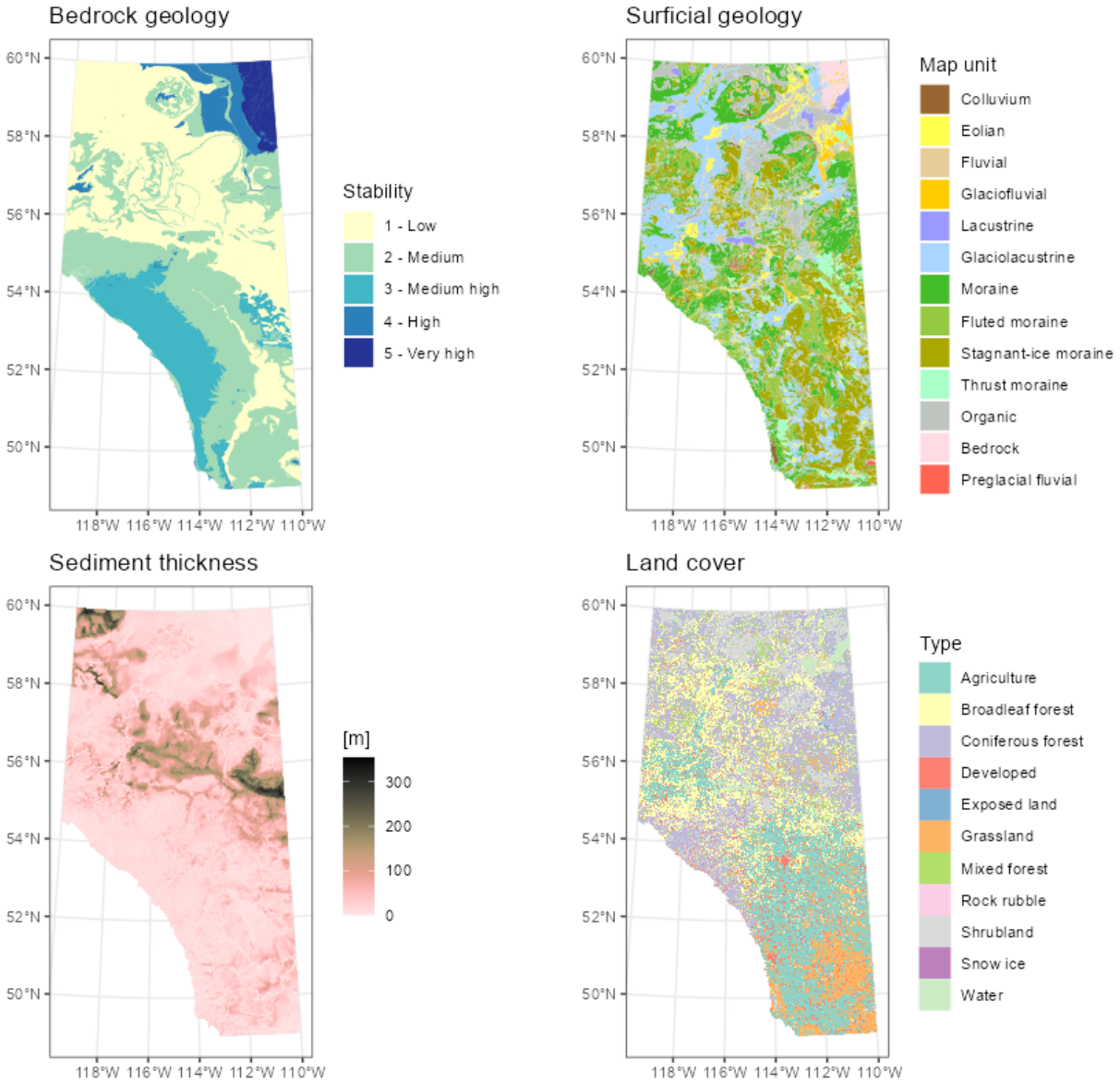

Figure 2. Bedrock geology, surficial geology (Fenton et al., 2013), sediment thickness (Atkinson et al., 2020), and land-cover (Castilla et al., 2014) data inputs for landslide susceptibility model. Bedrock geology is encoded as relative rock strength based on lithology and depositional environment (Pawley et al., 2016; modified after Prior et al., 2013).

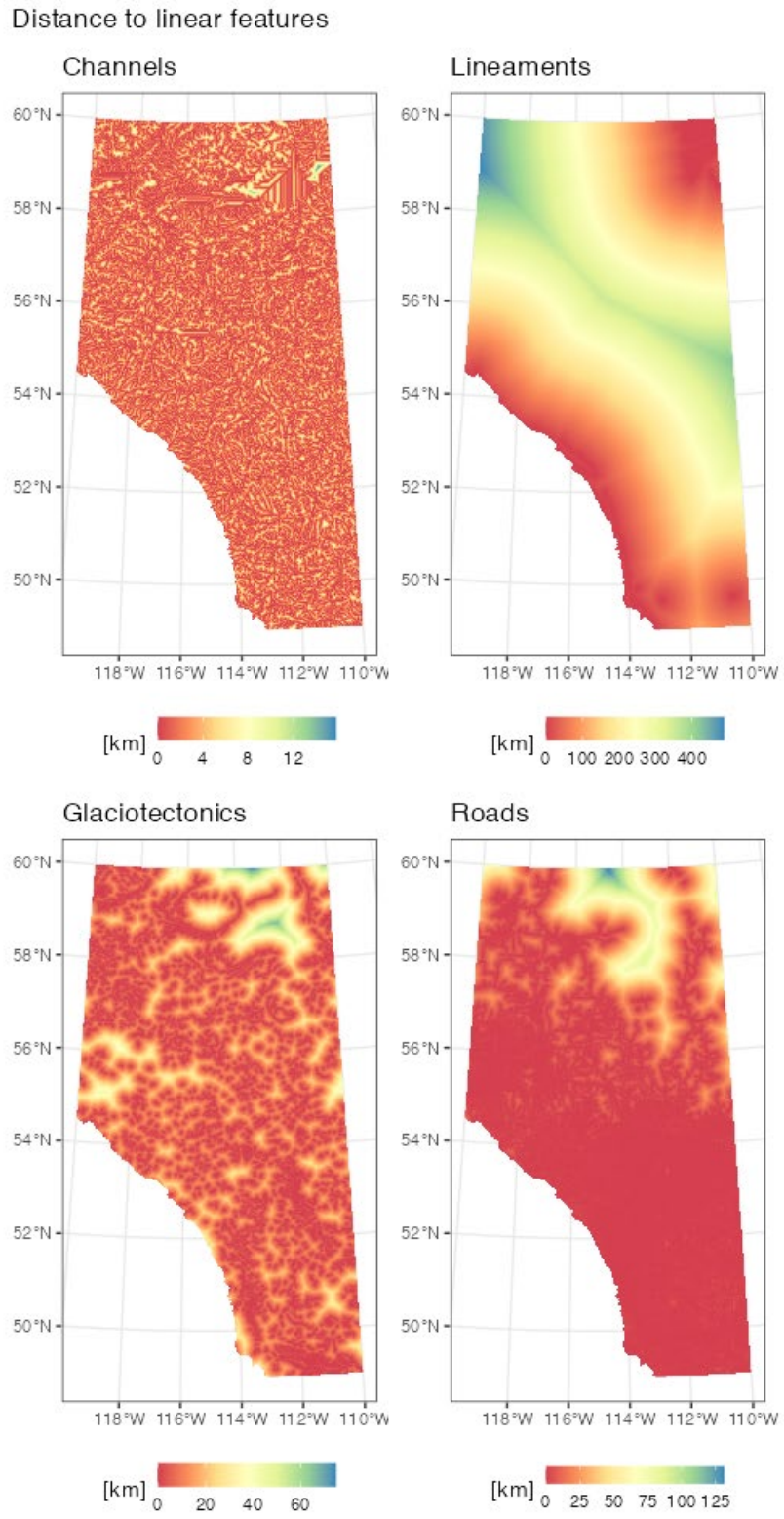

Figure 3. Two-dimensional Euclidean distance transforms to linear geological and landscape features including stream channels (example shown is for streams of Strahler order ≥7), regional structural lineaments (Prior et al., 2013), ridge lines of glacially deformed landforms (thrusts and moraines; glaciotectonics; Atkinson et al., 2014), and roads, included in landslide susceptibility model.

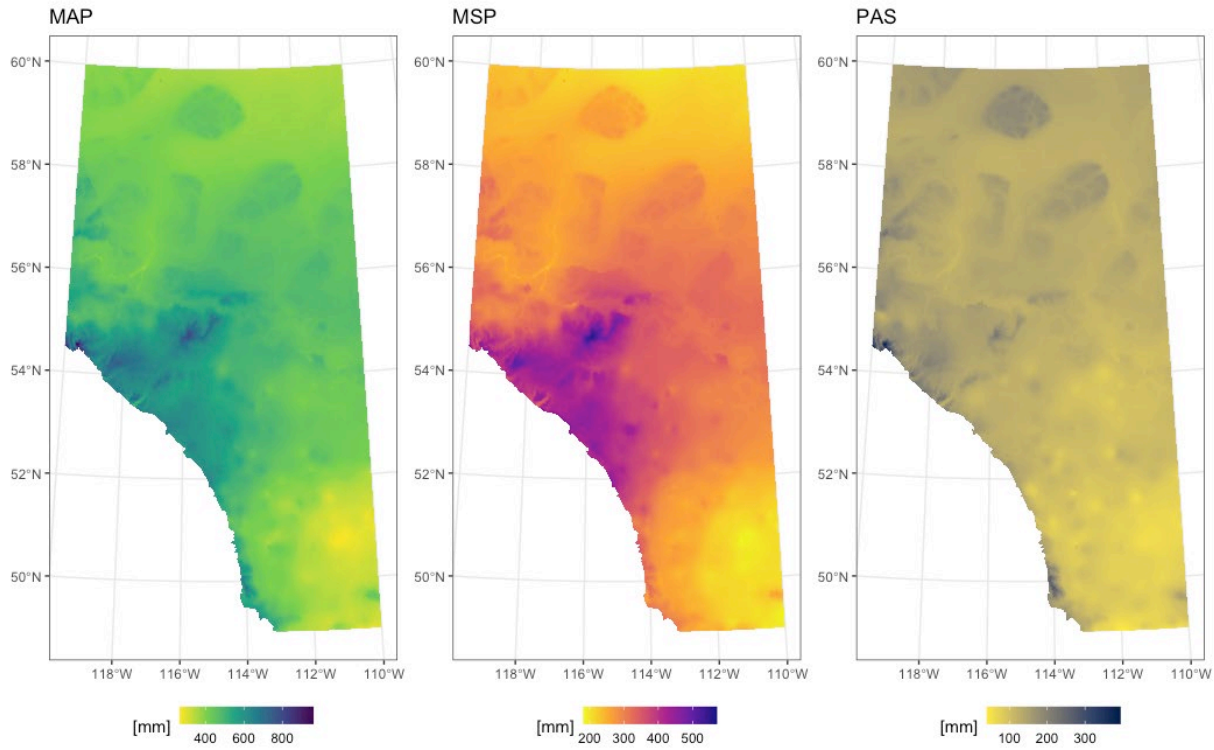

Figure 4. Precipitation variables from the ClimateWNA gridded datasets representing the 50-year averages (https://sites.ualberta.ca/~ahamann/data/climatewna.html; Wang et al., 2012), included in landslide susceptibility model. Abbreviations: MAP, mean annual precipitation; MSP, mean summer precipitation; PAS, precipitation as snow.

3.4 Terrain Features

Terrain analysis on the LiDAR DEM (Figure 5) was performed using libraries within System for Automated Geoscientific Analyses (SAGA)-GIS software (Conrad et al., 2015) within R via the 'Rsagacmd' package (Pawley, 2021). Standard land surface parameters consisting of slope angle, aspect, longitudinal curvature, and cross-sectional curvature were calculated from the LiDAR DEM using the Wood (1996) method. Aspect was decomposed into 'northernness' and 'easternness' using a sine or cosine transformation, respectively (Olaya, 2009). Topographic roughness was calculated using the vector ruggedness measure (VRM; Sappington et al., 2007), which assesses the magnitude of slope and aspect as a three-dimensional vector, as well as the terrain ruggedness index (TRI; Riley et al., 1999), which measures the difference in elevation between the centre pixel and its surroundings. The local terrain morphometric variables and topographic roughness variables, representing moving window-based methods, were calculated over multiple window radii (from 1 to 15) to incorporate varying scales of information. Terrain surface texture (Iwahashi and Pike, 2007) was used as an additional topographic roughness measure because it is based on calculating the density of pits and peaks in the DEM over a five-pixel radius and was visually found to delineate intensely gullied areas of terrain. Finally, geostatistical representativeness (Böhner et al., 2006) was used as an additional measure to describe terrain morphology and ruggedness. Representativeness describes the average variogram range or 'distance' where surrounding pixels are largely correlated/similar to the centre pixel, in a moving window analysis.

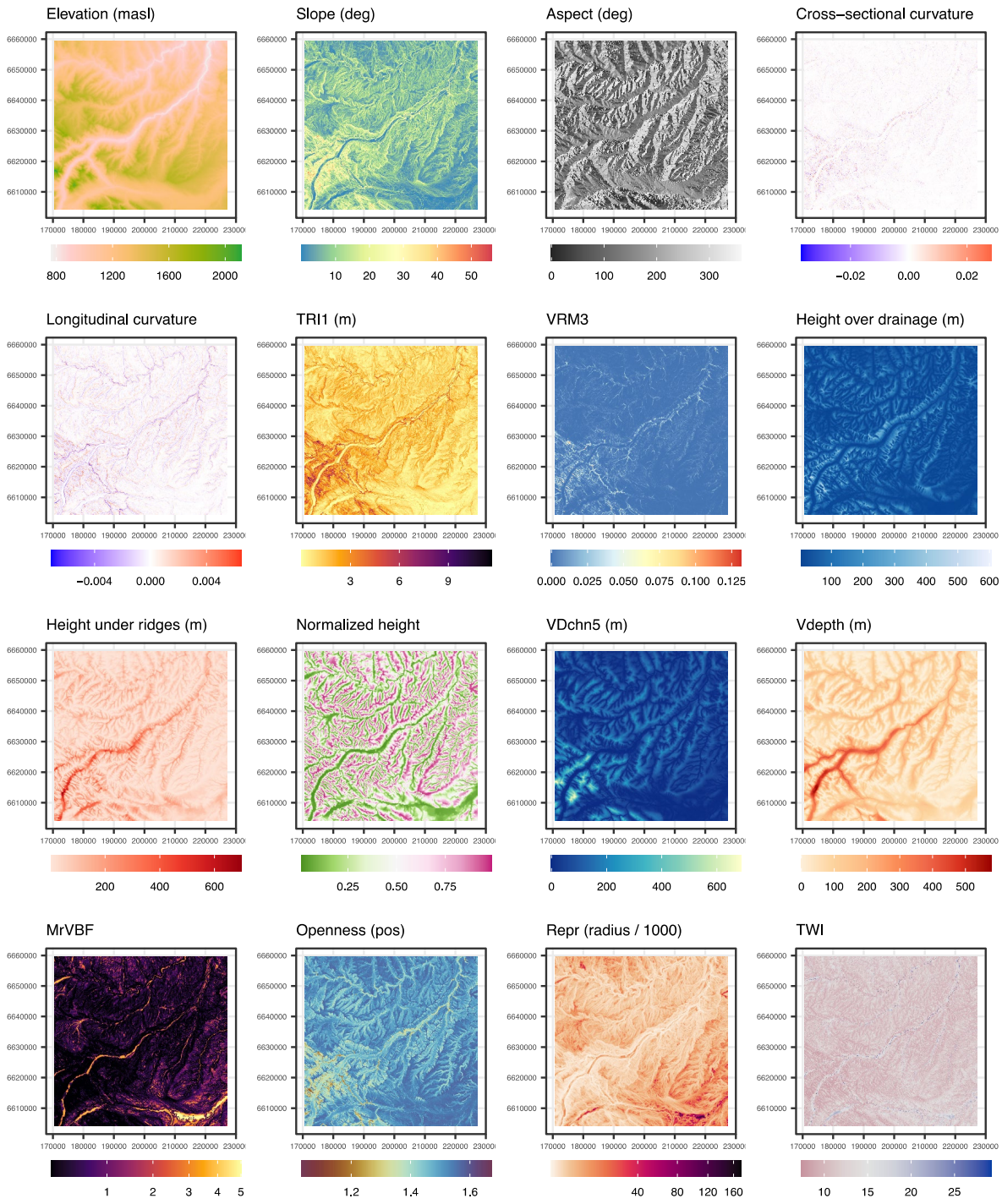

Figure 5. Terrain features used as predictors in the landslide susceptibility model. Note that the local morphometric variables (slope, aspect, longitudinal curvature, cross-sectional curvature) and topographic roughness variables (terrain ruggedness index [TRI], vector ruggedness measure [VRM]) were calculated over multiple moving window radii (not shown). All coordinates are shown in NAD83 10TM (EPSG: 3400) coordinate reference system, scale in metres. Abbreviations: deg, degree; MrVBF, multiresolution valley bottom flatness index; pos, positive; Repr, representativeness; TWI, topographic wetness index; V, valley; VDchn, vertical distance to channel network.

Regional morphometric variables quantify landscape-scale topographic relationships. Topographic openness (Yokoyama et al., 2002) was calculated to visualize regional topographic convexities and concavities. In the context of landslide susceptibility, topographic openness is related to the maturity of river valleys and gullies, where active erosion contributes to landslide activity. The topographic convergence index was also used to describe gullied areas, which tend to be the foci of landslides, based on the agreement of aspect direction of surrounding cells over a 10-pixel radius area (300 m at the model resolution). Two measurements of relative slope position were also calculated in SAGA-GIS (Conrad et al., 2015) based on the difference in surface elevations interpolated from channels and ridges in the DEM, resulting in estimates of vertical distance to channel networks (VDchn) and valley depth. The VDchn describes slope height above channels and is closely related to the driving forces of landslide initiation due to the potential energy available for downslope movement. Conversely, valley depth provides a quantification of the degree of fluvial incision below ridge and plateau elevations and is particularly relevant for predicting the landslide susceptibility of incised river valley walls. The VDchn was calculated relative to stream channels delineated from a hydrologically corrected version of the DEM. Only streams of 5, 6, and 7 Strahler orders were included. Similar variables that describe relative heights (height over drainage, height under ridges, normalized height; Conrad et al., 2015) based on generalized flow accumulation areas were included as additional measures because they tend to better highlight regional patterns in relief rather than height differences to localized channel lines. The multiresolution valley bottom flatness (MrVBF) index measures the flatness and lowness of terrain over multiple DEM resolutions and was used because it distinguishes lowlands and valleys from other sloping terrain (Gallant and Dowling, 2003). Finally, the topographic wetness index (TWI) was used to estimate the spatial distribution of soil moisture, based on the upslope contributing area and the local slope angle (Böhner and Selige, 2006). Given that soil saturation can reduce soil cohesion, topographic wetness is commonly used as a predictor in landslide susceptibility assessments.

3.5 Landslide Locations

3.5.1 Landslide Footprint Detection Inventory

Two sets of landslide inventory data were used for the project. The spatial prediction of landslide footprint extent used the same data as version 1 (Pawley et al., 2016), which was based largely on landslides depicted in surficial geology maps and published reports, and mapped based on LiDAR data. These landslide locations include polygons that were converted to points using random sampling within the polygon areas. These landslide locations do not contain any information in respect to the age or activity status of each landslide. This first inventory dataset is referred to as the ‘landslide footprint detection inventory’.

3.5.2 Landslide Susceptibility Inventory

The second dataset detailing landslide distribution (Figure 6) consists of locations where the timing of slope failure is approximately known and is confined to a historical time period (i.e., during the past 50–100 years approximately). These locations, published in AGS Digital Data 2022-0007 (Pawley et al., 2022c), were derived from several sources:

- Alberta Transportation reports of slope failures
- Alberta Energy Regulatory pipeline incidents that were reviewed and attributed to slope failures
- published reports and journal articles
- unpublished geotechnical reports provided by Canadian National Railway Company as part of previous landslide mapping in the Peace River region (Morgan et al., 2012)
- Alberta Geological Survey field site observations
- the City of Edmonton’s Open Data Portal reports of closures to roads and trails due to landslides
- other local sources of information, such as local news articles

- Sentinel-1 SAR images acquired from 2017 to 2021; from the images, InSAR ground deformation rates were processed using the software developed at Natural Resources Canada, Canada Centre for Mapping and Earth Observation, which is based on the InSAR processing software developed by GAMMA Remote Sensing AG and time-series multidimensional small baseline subset (MSBAS) software developed by Samsonov and d'Oreye (2017)
- sets of multitemporal satellite and aerial imagery, including openly available Google Earth and Bing imagery, as well as high-resolution aerial images acquired in 2000–2001 and SPOT 6/7 satellite images acquired between 2013 and 2020.

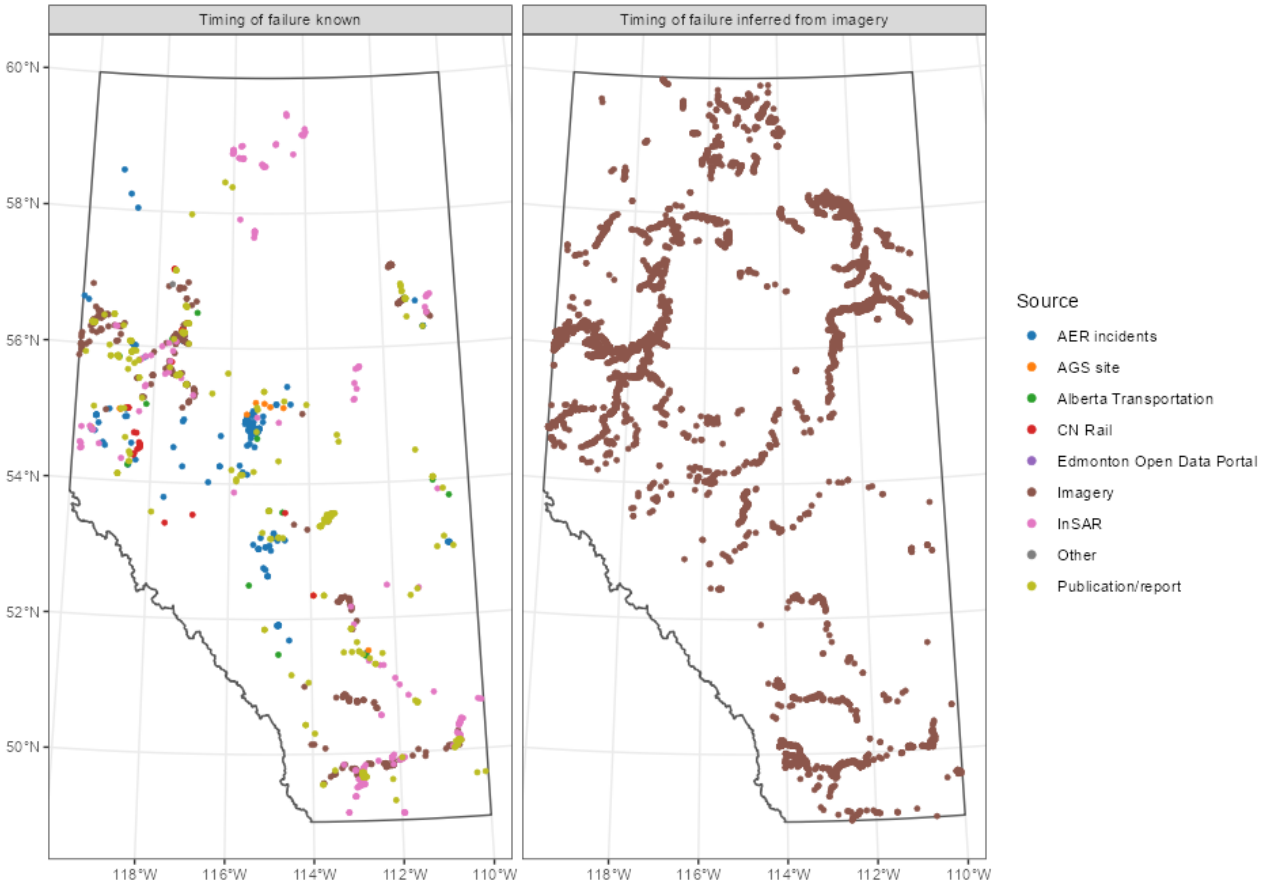

Figure 6. Landslide locations in the landslide susceptibility inventory categorized by data source. The left panel shows the locations of landslides where the timing of movement is known based on information from reports, InSAR ground deformation data, and changes in multitemporal imagery. The right panel shows landslide locations that are inferred to have been historically active based on visual criteria in imagery. Abbreviations: AER, Alberta Energy Regulator; AGS, Alberta Geological Survey; CN Rail, Canadian National Railway Company; InSAR, interferometric synthetic aperture radar data.

Although the timing of the slope failures within the compiled data is known, the timing of movement is not as well defined for locations obtained from interpretation of multitemporal imagery. For these data, each location was attributed based on whether movement was observable directly on different vintages of imagery, or whether it was inferred based on qualitative criteria. Several criteria were used to identify whether a landslide showed 'recent' (during the past 50–100 years approximately) evidence of movement:

- presence of toe bulges into rivers and streams, which otherwise would have been eroded if the landslides were relict
- evidence of freshly exposed scarps or ground cracks within the landslide mass or around its margins, observable in very high resolution imagery
- evidence of fresh flow-like material within broader areas of complex earthslides and flows
- presence of a high density of sag ponds covering the slope; it is assumed that, over time, most sag ponds would infill or drain if all landslide movement were to completely cease

3.5.3 Landslide Downslope Area Delineation

For most landslides in the landslide susceptibility inventory, the landslide location is represented by a single point within the upper/depletion area of the landslide. However, any terrain that is immediately downslope of these locations is also susceptible to slope failure. To incorporate some of these areas within the model, a procedure was used to isolate the downslope areas:

1) topographically inverting the LiDAR DEM data
2) using the multiple flow direction (MFD) hydrological flow accumulation algorithm on the inverted DEM to obtain the downslope areas
3) masking flat areas, that is, river channels and lakes that are immediately at the base of the slope

This procedure in many cases provided a reasonable approximation, or a slight underestimate, of the total failing area (Figure 7) and allowed sampling of the general failing area of terrain even when the landslides are mapped using only a single point. A potential improvement in future work could be to map the landslide headscarps as lines and then apply the downslope method, which would more precisely capture the landslide bodies without having to map every landslide as a polygon, which would be very time-consuming at the scale of the model.

4 Machine Learning

4.1 Modelling Approach

Landslide susceptibility modelling was performed using the R statistical language (R Core Team, 2020). The susceptibility is based on the statistical similarity of the predictors relative to the two endmembers, consisting of the pixels within the landslide areas, augmented by a random background sample. The nested modelling procedure (Figure 8) is based on three steps:

1) To distinguish landslides from other nonlandslide terrain, the landslide footprint detection inventory (consisting of landslide pixels of any age or activity level) was augmented by a random background sample obtained from the entire model area. The background sample was used as a surrogate for a nonlandslide class. This is a commonly used approach in landslide susceptibility investigations because known 'nonlandslide susceptible' locations do not physically exist. Furthermore, although the background sample could include some landslides (false negatives), the total area of Alberta that contains landslides is relatively small, which justifies the use of this sampling strategy. The number of background locations was made to be equal to the number of landslide locations to create a balanced training dataset.

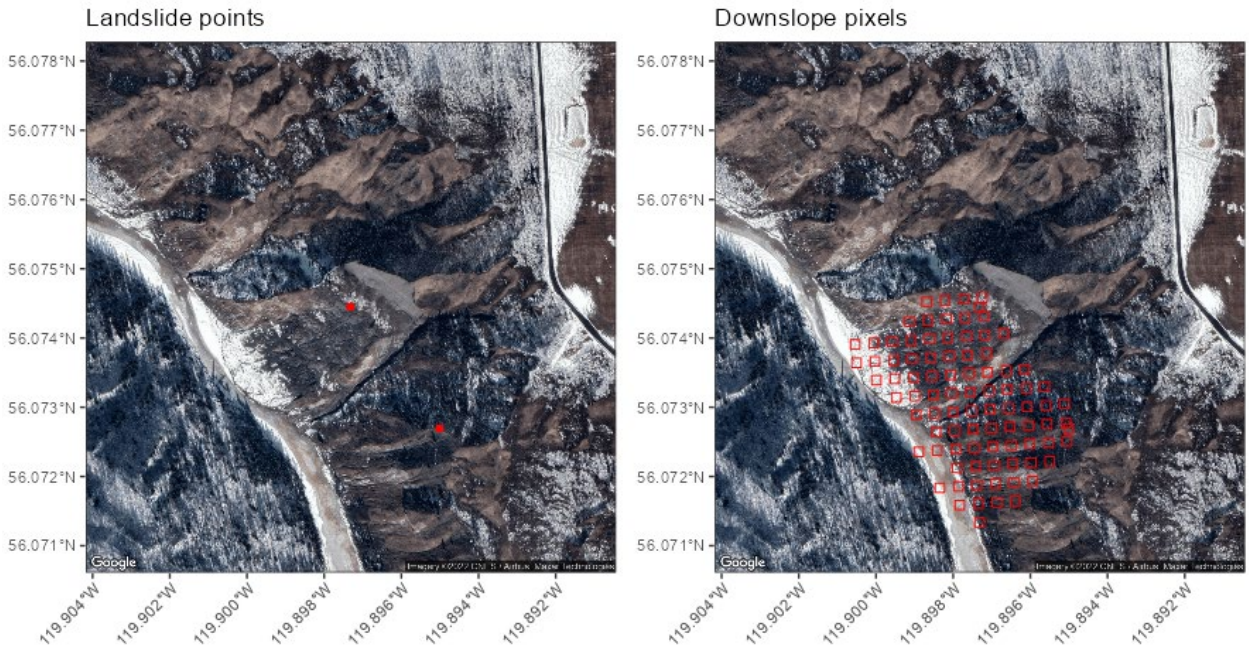

Figure 7. An example of two landslide points (left) and the downslope pixels (right) that were sampled as part of the landscape susceptibility model. Imagery ©2022 CNES/Airbus Maxar Technologies.

2) The landslide footprint detection inventory and statistical background sample was used within a binary classification model to predict the spatial distribution of all landslide terrain, irrespective of age or activity status.
3) A second model was developed to estimate the susceptibility of the landslide terrain, delineated in step 2, to future slope failures. This model used the training data based on the landslide susceptibility inventory. These data were augmented with a random sample taken from within the predicted landslide footprint extent but masking out the historically failing areas of terrain. The sample of the remaining pixels is considered to approximate a 'relict' landslide class, which is used to distinguish historically failing terrain from terrain that is apparently relict/stable. These data are used to evaluate the topographic, climatic, and geological conditions in areas that have active or historically active landslides, relative to landslide terrain overall.

An initial step of data exploration was used to identify potential statistical transformations that needed to be applied to the predictors, or whether any predictors should be removed. These transformations were applied to the data as part of the preprocessing recipe (Table 1) to ensure that the transformations were applied both to the training data during model training, and the raster data during prediction. The preprocessing recipe consisted of converting categorical data types stored as integer values in the raster grids into their corresponding categorical classes as factor variable types, reclassifying some categories, pooling infrequently occurring categories, and creating new derivative variables.

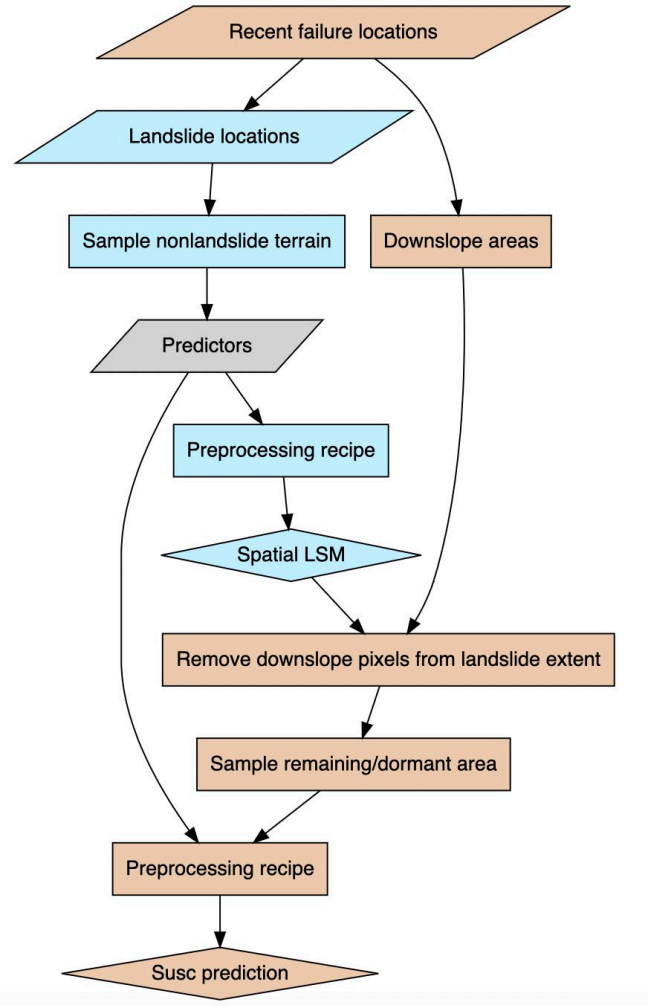

Figure 8. Modelling steps and workflow. The blue-coloured steps signify steps that are associated with the landslide footprint detection model; the salmon-coloured steps are associated with the landslide susceptibility model (LSM). Abbreviation: Susc, susceptibility.

Table 1. Steps within the preprocessing recipe for data transformation.

Number	Operation	Type	ID
1	Step	rm	Remove variables
2	Step	num2factor	Land cover to factor
3	Step	num2factor	Bedrock to factor
4	Step	mutate	Pool bedrock categories
5	Step	mutate	Pool land cover categories
6	Step	mutate	Create climate derivatives
7	Step	other	Pool infrequent categories
8	Step	novel	Add a novel category
9	Step	ordinalscore	Bedrock factor to ordinal score

4.2 Machine Learning Algorithms

The landslide footprint detection model used the XGBoost algorithm (Chen and Guestrin, 2016), which is based on the gradient boosted trees approach. Gradient boosted trees represent an ensemble decision tree approach, where predictive accuracy is improved using an additive, forward stepwise process. During this process, additional decision trees are fitted to model observations that were not accurately predicted by the previous tree, that is, it iteratively fits to the model residuals. During each iteration, the algorithm determines the gradient in which it needs to improve the modelled fit to the data and fits a tree to the gradient of the loss function to reduce the loss by a relatively small step.

A disadvantage of boosted tree methods is that they tend to create abrupt spatial changes in the predicted probabilities, sometimes appearing as visible artifacts and lines in the predicted class probabilities. Because the landslide susceptibility model uses the class probabilities as a surrogate for the landslide susceptibility, the extremely randomized tree algorithm was used for this model instead of boosting. Extremely randomized trees is a variant of Random Forests, which is an ensemble decision tree method that constructs a 'forest' of poorly correlated decision trees to overcome the problems of using a single decision tree, which tend to strongly overfit the training data. The trees in a Random Forest model are forced to be uncorrelated because only a random subset of the training data is used to build each tree (termed bagging), and only a random subset of predictor variables is allowed to be available at each node split. The extremely randomized trees algorithm takes this concept further by using a random splitting rule at each node, where the decision is based on the best of a small number of randomly chosen thresholds in the predictors, which further increases the variance of the individual tree's predictions across the forest. In practice, this has a 'smoothing' effect on the model's predictions relative to using a traditional Random Forest approach.

4.3 Quality Control

The performance of machine learning models is commonly evaluated against holdout data using resampling strategies such as k-fold cross-validation. However, with spatial data, the presence of spatial autocorrelation can lead to overly optimistic performance estimates when random (nonspatial) sampling is used for partitioning into training and testing datasets. Although landslide susceptibility mapping based on a single point per landslide is cited as one approach to mitigate this, individual point locations can still be autocorrelated. Furthermore, in the revised approach, all pixels downslope of each landslide point were used, and these observations will be highly spatially correlated.

Spatial cross-validation using spatial blocks was chosen as a resampling strategy to mitigate these issues. The data was divided into spatially discrete rectangular blocks and then the blocks were allocated to cross-validation folds. The size of the blocks was determined prior to modelling by estimating the variogram range of each raster predictor at the training data locations and taking the median of the ranges across the predictors as the block size.

This resulted in the training data being partitioned into 105 discrete spatial blocks (Figure 9), and these were allocated within five-fold cross-validation resamples. The same spatial blocking strategy was also used for hyperparameter tuning, which typically uses a holdout set or cross-validation to select the most optimal parameter values for the model. Because selecting the most optimal hyperparameters on the same data that is used to evaluate model performance can lead to overly optimistic estimates, a nested spatial block cross-validation approach was used. In this approach, an outer resampling loop is used to partition the training data into blocks that are assigned to five folds, with k-1 folds used to train the model and the kth fold used to evaluate model performance. Then within each fold, the remaining k-1 blocks are partitioned again into spatial blocks and allocated to an inner five-fold resample to select the best hyperparameters.

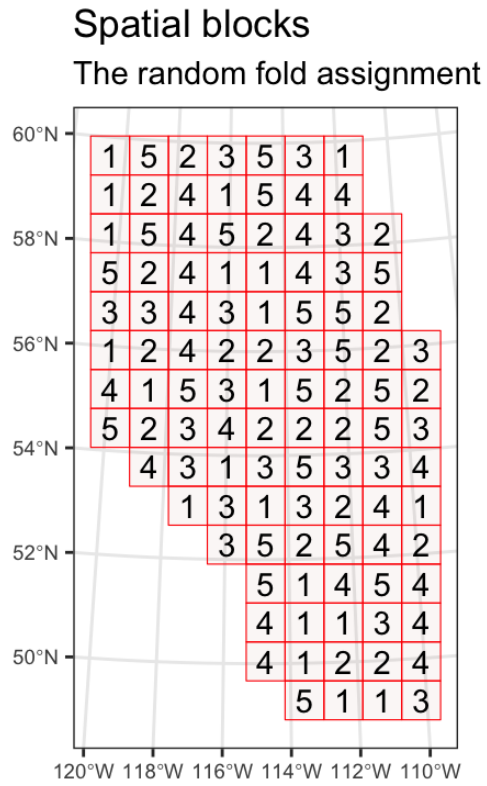

Figure 9. Example of spatial block sizes based on the median variogram ranges of the predictors, allocated to a five-fold resampling strategy. The number in the block shows the k-fold that each spatial block of data is allocated to. For k = 1, k = {1, 2, 3, 4} are used to train the model and the remaining fold is used to evaluate model performance. This is repeated until all k-folds have been used for both training and testing, that is, five repetitions.

Model performances were evaluated using accuracy, precision, recall, and F-measure (F1) scores. Accuracy is the proportion of correctly identified landslide and background observations. Recall (also termed sensitivity or true positive rate) is the proportion of true positive (landslide) predictions relative to the total number of actual positives, that is, TP/(TP+FN) where TP is the total number of true positives and FN is the total number of false negatives. Recall indicates how well the positive class can be predicted. Precision is the proportion of true positives relative to the total number of predicted positives, that is, TP/(TP+FP) where FP is the total number of false positives. Precision describes the relevance of the model, that is, the ability of the model to predict only relevant observations. The F-measure score summarizes precision and recall into a single estimate based on their harmonic mean.

Precision and recall depend on the cutoff used to categorize the probabilities into the positive and negative classes. A cutoff of 0 would yield a perfect recall rate (all positive observations would be correctly identified) but would yield a precision score of 0 (because all negative observations would be misclassified as positive). Thus, the overall model performance was also evaluated using a cutoff independent metric, based on the area under the receiver operating characteristic curve (AUC-ROC). The AUC-ROC represents the area under the curve formed by the true positive rate and false positive rate relative to every cutoff threshold between 0 and 1.

5 Data Exploration

5.1 Local Terrain Characteristics

Density ridge plots (Figure 10) show the distribution of values in the historical landslide and relict classes across the local terrain features and topographic roughness measures, using multiple window radii. The ridge plots show that only limited separability occurs between the classes, although the separability increases for large window sizes. This indicates that historical landslides have similar morphology as relict landslides, albeit the documented historical landslides have slightly increased roughness characteristics potentially reflecting a 'fresher' morphology.

Aspect has been implicated as having a role in landslide susceptibility because north-facing slopes are shaded in the northern hemisphere for the warmest parts of the day and are therefore characterized by wetter slope conditions, which promotes slope instability. Density ridge plots of aspect in the training data, transformed to the vector magnitude of the northerly direction (Figure 11), show that more landslides occur on both north- and south-facing slopes compared to west- and east-facing slopes. This reflects that most rivers in Alberta drain approximately eastwards. Additionally, a slight increase in the probability density of landslides occurring on south-facing slopes, rather than north-facing slopes, is observable in the data. In the absence of any established physical mechanisms, this is indicative of a mapping bias because south-facing slopes have thinner vegetation cover, making landslides more easily observable. Owing to the lack of an apparent physical connection between landslide density and aspect, as well as the potential exaggeration of mapping biases, the aspect-based variables were excluded from the model.

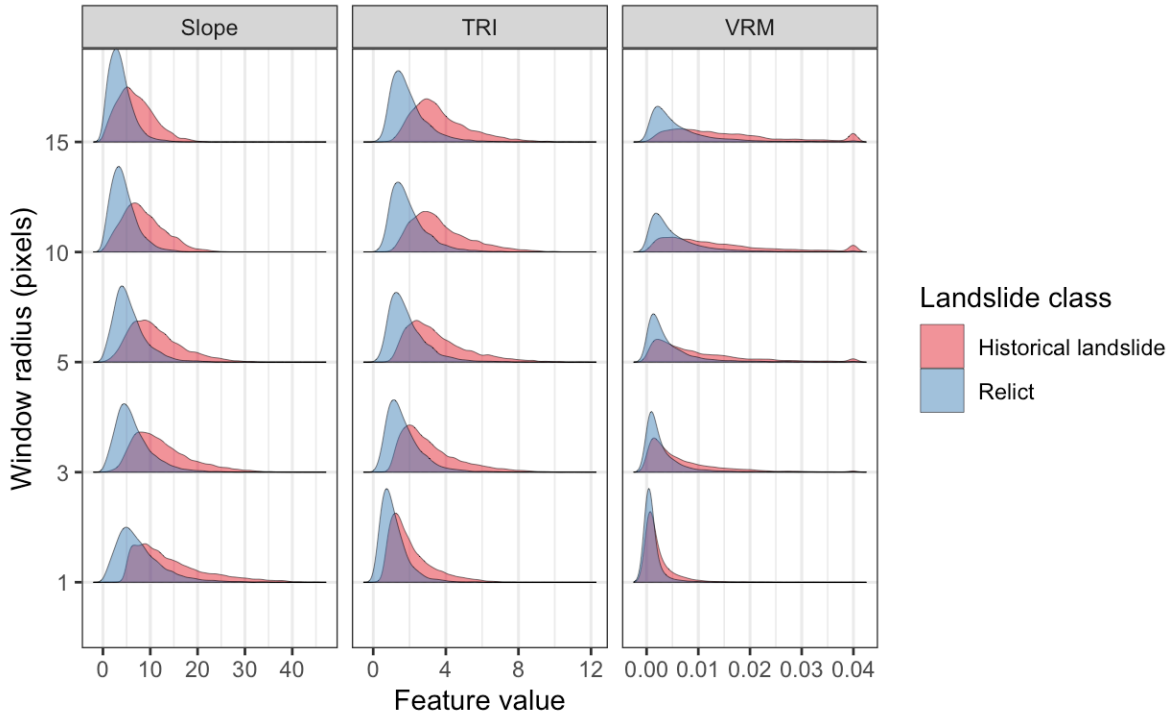

Figure 10. Density ridge plots for the local morphometric and topographic roughness variables, calculated over multiple moving window sizes. Abbreviations: TRI, topographic roughness index; VRM, vector ruggedness measure.

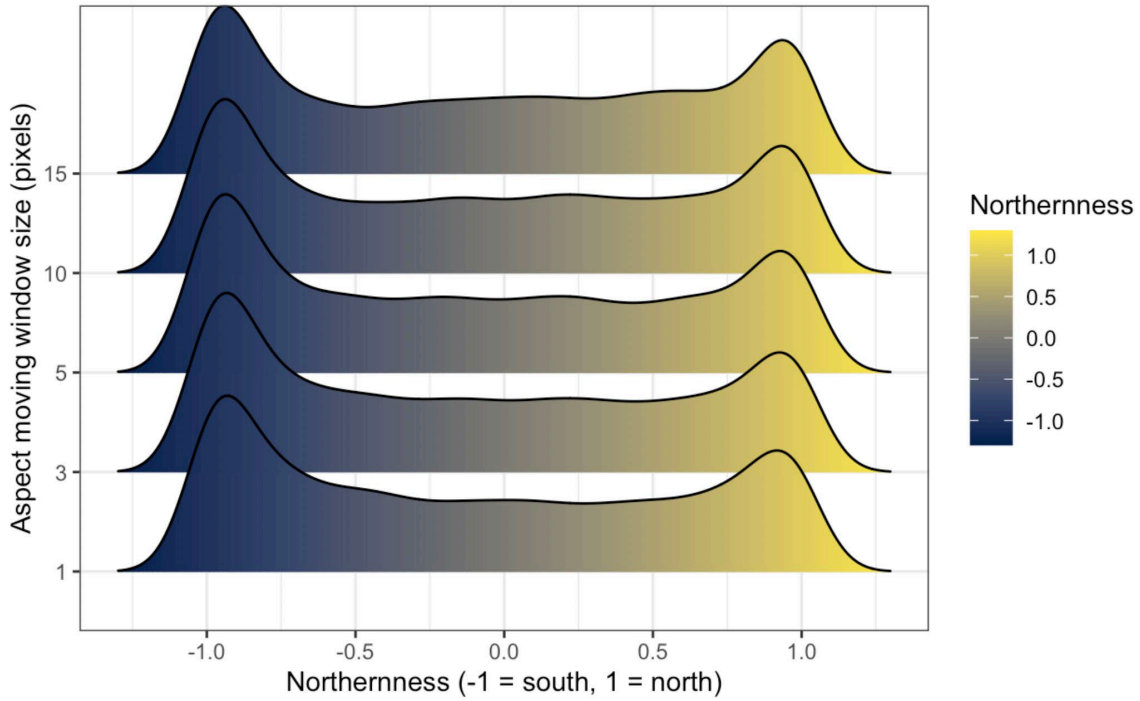

Figure 11. Density ridge plots for aspect, transformed to the strength of the northerly direction. North-facing slopes have a value of 1, and south-facing slopes have a value of -1. The density plots show that landslides are more prevalent on north- and south-facing slopes, which is expected because most major rivers in Alberta drain approximately eastwards. However, the greater prevalence of landslides on south-facing slopes relative to north-facing slopes suggests a mapping bias, because landslides are more easily observable on south-facing slopes due to thinner vegetation cover.

5.2 Topographic Position

Pairplots were created to show the distribution of values in the topographic position–related variables (Figure 12). The pairplots show that individually (diagonal panels) only small to moderate levels of separability occur between the historical landslide and relict classes. However, when features are combined, separability is increased. This indicates that interactions between features potentially provides some separation of the classes and provides some intuition as to how a machine learning model may potentially discriminate between the classes through many complex interactions between variables.

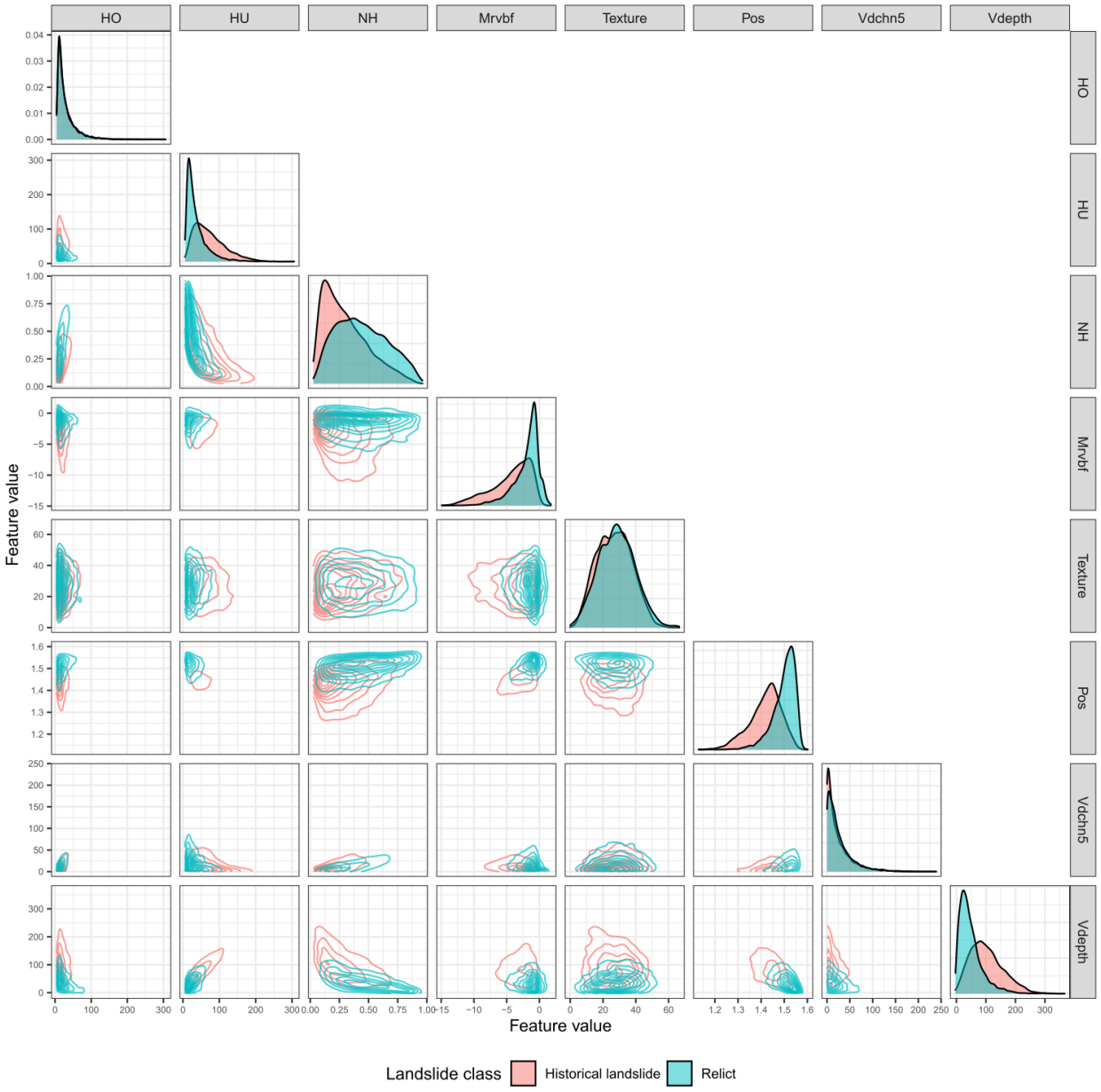

Figure 12. Pairplots of topographic position–related variables. The nondiagonal plot elements show the bivariate distributions of the historical landslide and relict classes. The diagonal plot elements show the distributions of individual features in the historical landslide and relict classes. The features are abbreviated as HO, height over drainage; HU, height under ridges; NH, normalized height; Mrvbf, multiresolution valley bottom flatness index; Texture, terrain surface texture; Pos, positive topographic openness; Vdchn5, vertical distance from channels with Strahler order ≥5; Vdepth, valley depth.

5.3 Distance-Related Features

Boxplots of the distance-related linear features (Figure 13) show a moderate degree of separability between the classes, particularly with distance to the channels of streams with larger Strahler orders. This indicates that for at least the historical landslides related to river erosion, the combination of topographic position and stream channel distance variables offers promise for predicting susceptibility. In contrast, the spatial distribution of historical landslides does not appear to be associated with proximity to glaciotectonic structures (ridges), structural lineaments, or roads. Rather, distance to roads shows the opposite effect, where most historical landslides are situated far away from roads. Although initially counterintuitive, because slope modifications from roadcuts and embankments can trigger landslides, at a provincial scale, most roads in the Alberta Plains are situated on low-lying terrain and roads only encroach on landslide terrain in limited situations. Additionally, roadbuilders would prefer to avoid areas of obvious active landslides, and the history of roadbuilding in Alberta largely covers the past 50–100 year historical landslide interval.

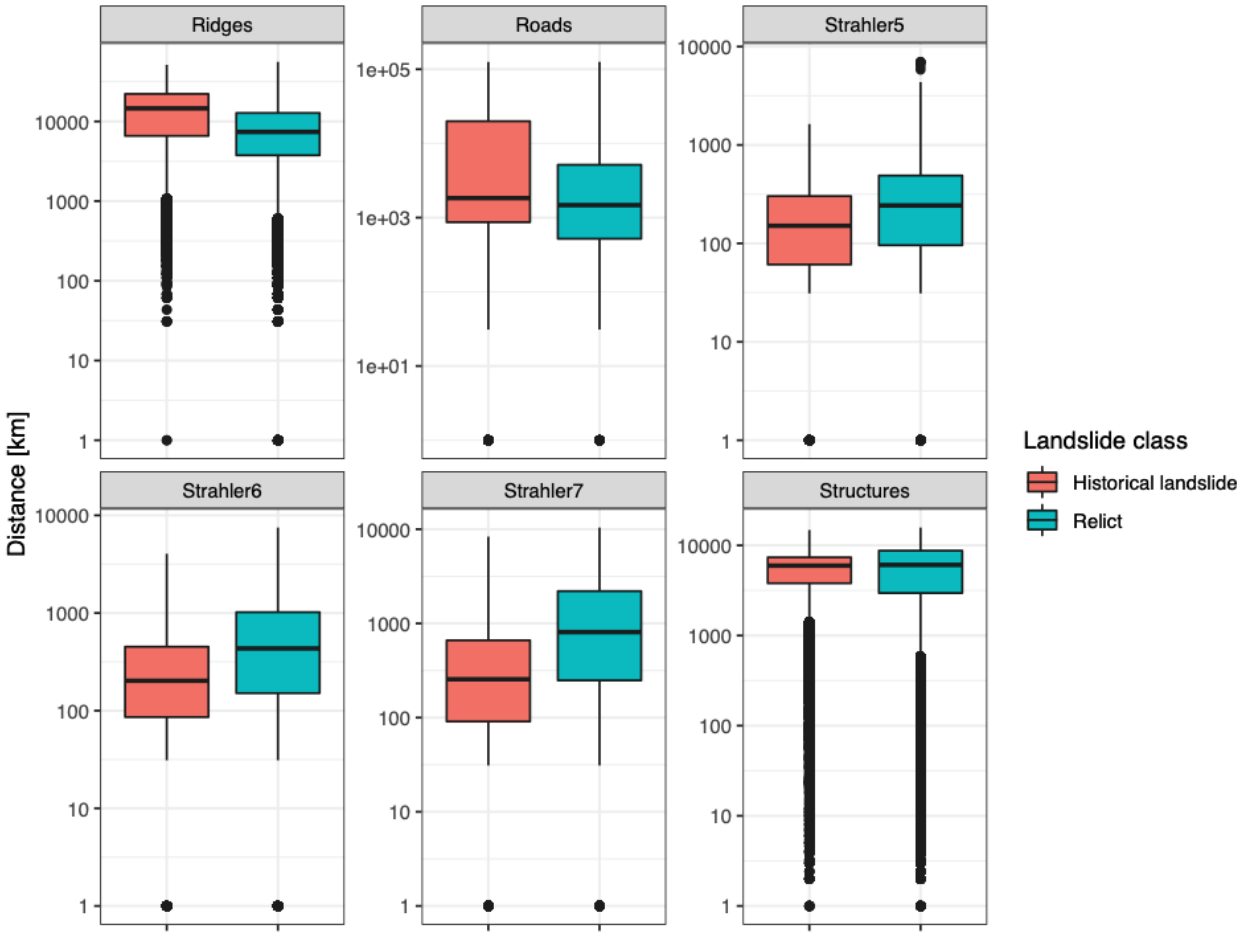

Figure 13. Boxplots of Euclidean distance transform variables to linear geological and landscape features. Abbreviations: Ridges, glaciotectonic ridges; Strahler5, Strahler order 5 river; Strahler6, Strahler order 6 river; Strahler7, Strahler order 7 river; Structures, structural lineaments.

5.4 Precipitation

Kernel density plots of precipitation (Figure 14) initially appear to show that no obvious relationship exists between the precipitation variables and landslide density, rather the data appear to show a counterintuitive relationship that more landslides occur in drier climates. This apparent inverse relationship is explained by the precipitation signal being largely influenced by elevation, and many landslides are mapped along river valleys, which tend to occur at the lowest elevation in a region. When the precipitation variables are normalized by elevation, the density plots (Figure 14) show a moderate influence of precipitation on landslide density, with regions that have similar elevation values but wetter climates having a greater density of landslides. On this basis, these normalized precipitation variables were added to the model to provide a more direct link to climate.

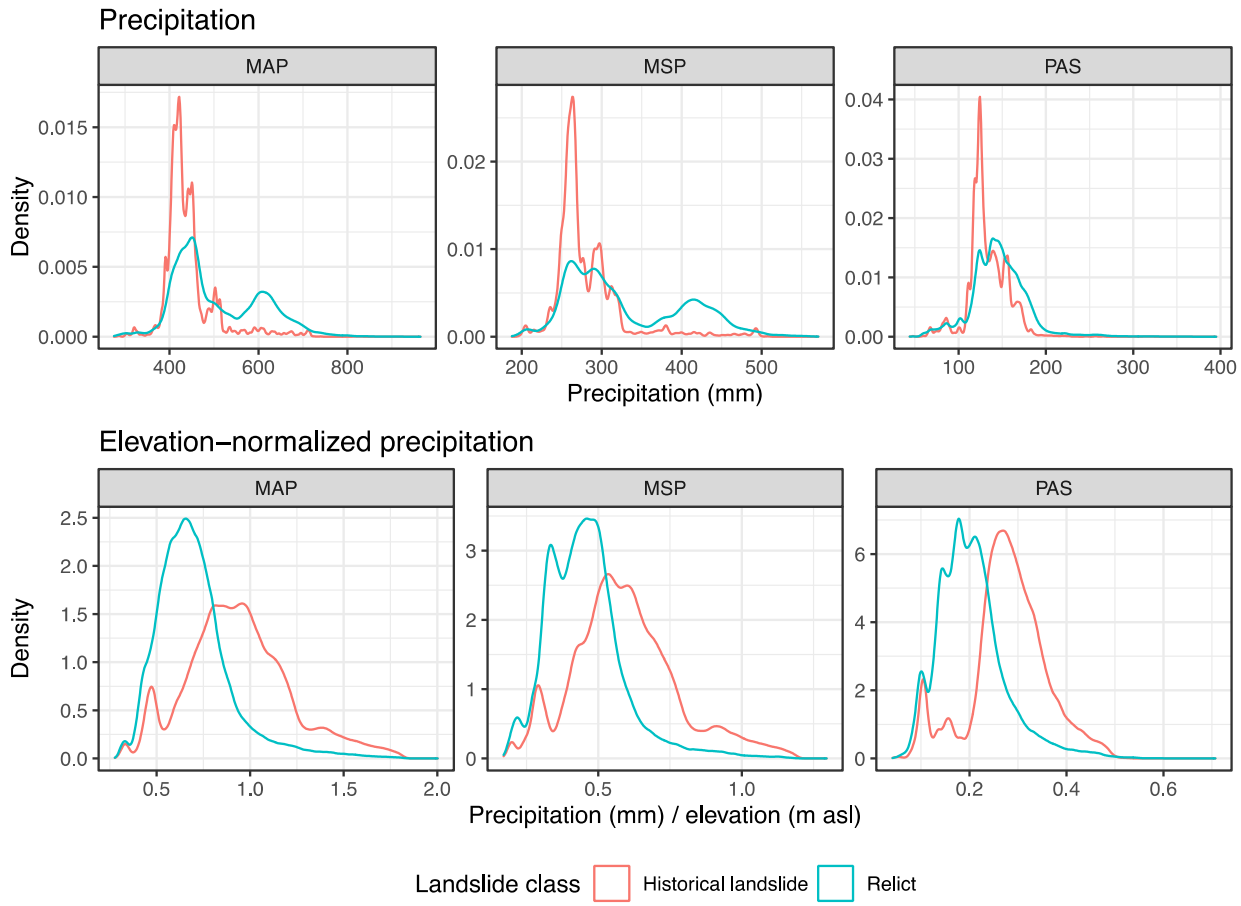

Figure 14. Kernel density plots (effectively smoothed histograms) of precipitation (top) and elevation-normalized precipitation (bottom) variables. The x-axis shows the value of each variable and the y-axis is the probability density, where the y-axis values are scaled so that the area under the curve is equal to 1. After normalizing precipitation by elevation, precipitation does appear to exert a moderate influence on landslide occurrences, with wetter areas at approximately the same elevation containing more landslides. Abbreviations: MAP, mean annual precipitation; MSP, mean summer precipitation; PAS, precipitation as snow.

5.5 Geology and Land Cover

Landslide abundances relative to categories in the geological and land-cover maps (Figure 15) show that bedrock geology, encoded as a relative rock strength, has a strong relationship to landslide abundance. The low rock strength category has the highest proportion of landslides, the medium category has a near equal proportion of landslides and nonlandslides (statistical background class), and the medium-high category contains very few landslides. The other two categories contain very little data, and consequently, these categories were pooled with the medium category to reduce the number of categories because large numbers of categorical variables can reduce the performance of tree-based machine learning models.

Land-cover type does not appear to show much relationship with landslide occurrences. The large proportion of landslides occurring in the water category reflects the low resolution of the land-cover data, in that some landslides mapped close to the edges of rivers are spatially falling into the water category. Based on the lack of obvious relationships between land-cover and landslide abundance, categories in the land-cover map were pooled into a smaller number of categories by grouping forest types and open-land types (e.g., shrubland, grassland, agriculture).

Surficial geology appears to show a strong relationship with landslide abundances. However, the majority of historical landslide class observations occur within the C (colluvium) or F (fluvial) map categories. Because the footprint of landslides has already been accurately established from the spatial prediction, the role of surficial geology appears to be limited and this variable was dropped from the model.

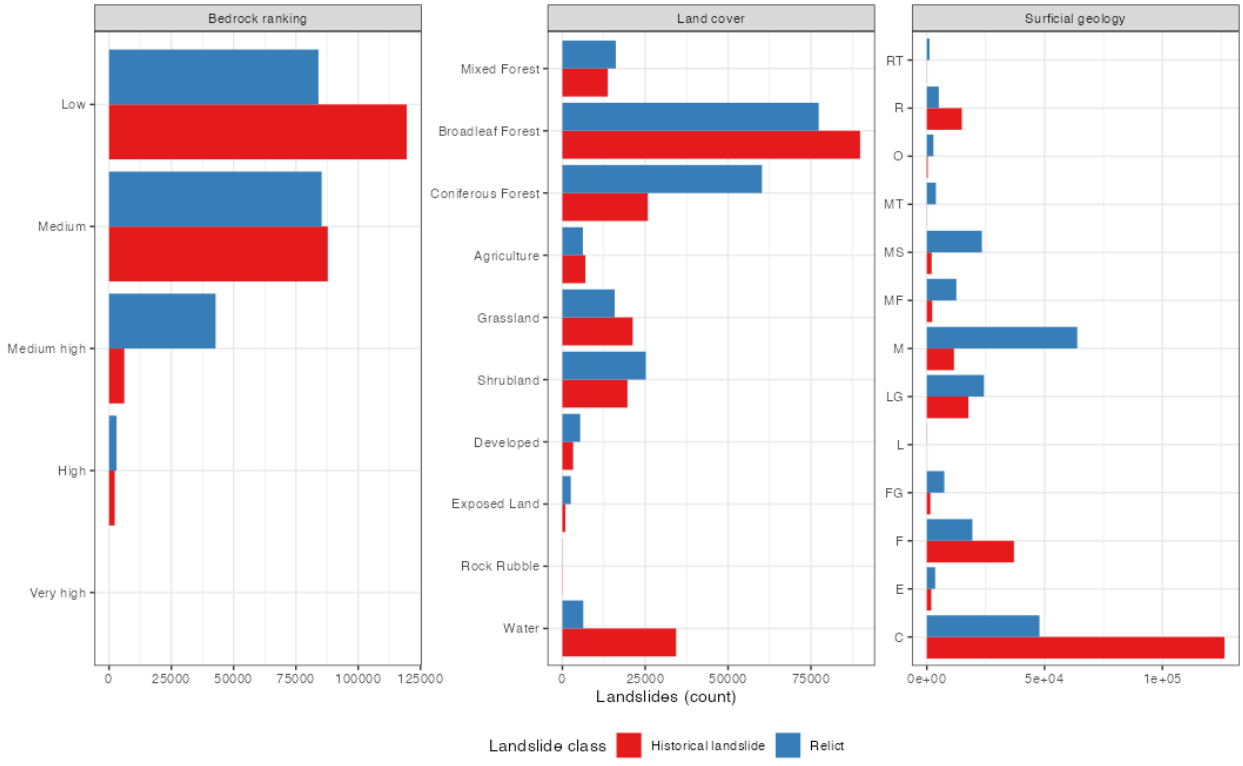

Figure 15. Bar plots of the number of landslides occurring in each category of the inputted geological and land-cover maps. Abbreviations: Bedrock ranking, ranking of bedrock strength; C, colluvium; E, eolian; F, fluvial; FG, glaciofluvial; L, lacustrine; LG, glaciolacustrine; M, moraine; MF, fluted moraine; MS, stagnant-ice moraine; MT, thrust moraine; O, organic; R, bedrock; RT, preglacial fluvial.

6 Results

6.1 Landslide Footprint Detection Model

The XGBoost spatial prediction model (i.e., the landslide footprint detection model) achieved an overall high accuracy of 94% and a very high AUC-ROC score of 0.98. The sensitivity of the classification accuracy, relative to the probability cutoff, was determined by examining precision, recall, F-measure, and accuracy for a range of cutoff thresholds (Figure 16). Precision and recall scores are equal at a threshold of 0.65, that is, the equal error rate (EER). However, the accuracy and F-measure scores are almost constant between cutoff thresholds ranging from ~0.35 to ~0.5. Consequently, the default cutoff threshold of 0.5 was retained to classify terrain into the landslide and background/nonlandslide classes.

6.2 Landslide Susceptibility Model

The parameters for the extremely randomized trees model (i.e., landslide susceptibility model) were tuned using the five-fold spatial block cross-validation approach, and the optimal hyperparameters were selected based on the parameters that yielded the maximum average AUC-ROC score. Model performance was best when approximately 33 predictors were available for selection at each node split, and when the minimum node size, which is the minimum number of observations required to form a leaf node, is 50, which will force slightly shorter trees (Figure 17). However, the overall difference in performance was very small.

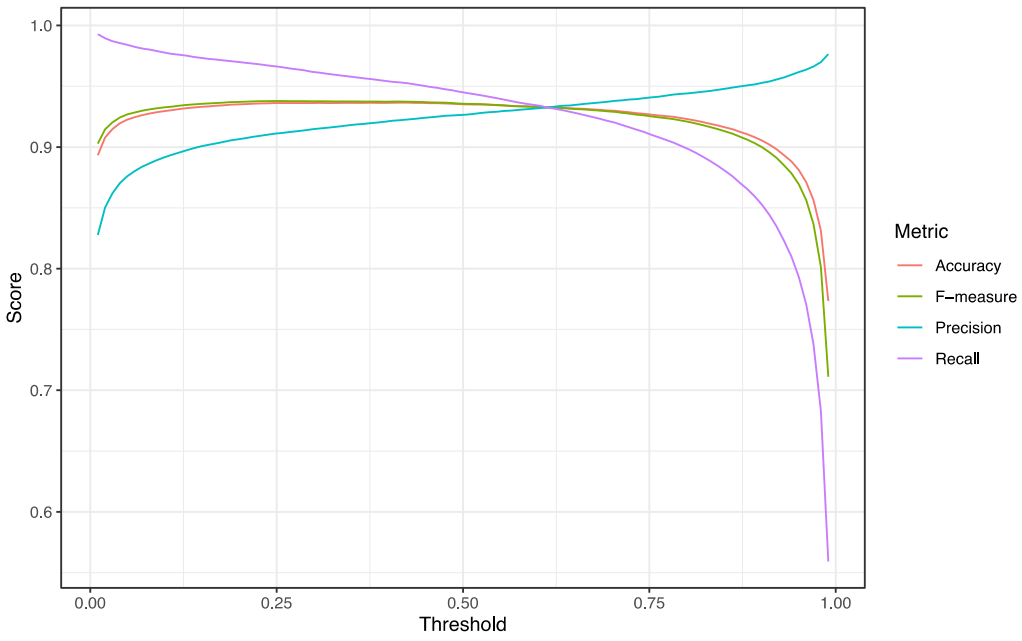

Figure 16. Accuracy, F-measure, precision, and recall scores for the spatial prediction of total landslide terrain extent from the landslide footprint detection model. The accuracy and F-measure scores show an optimal plateau between cutoff thresholds of ~0.35 and ~0.5.

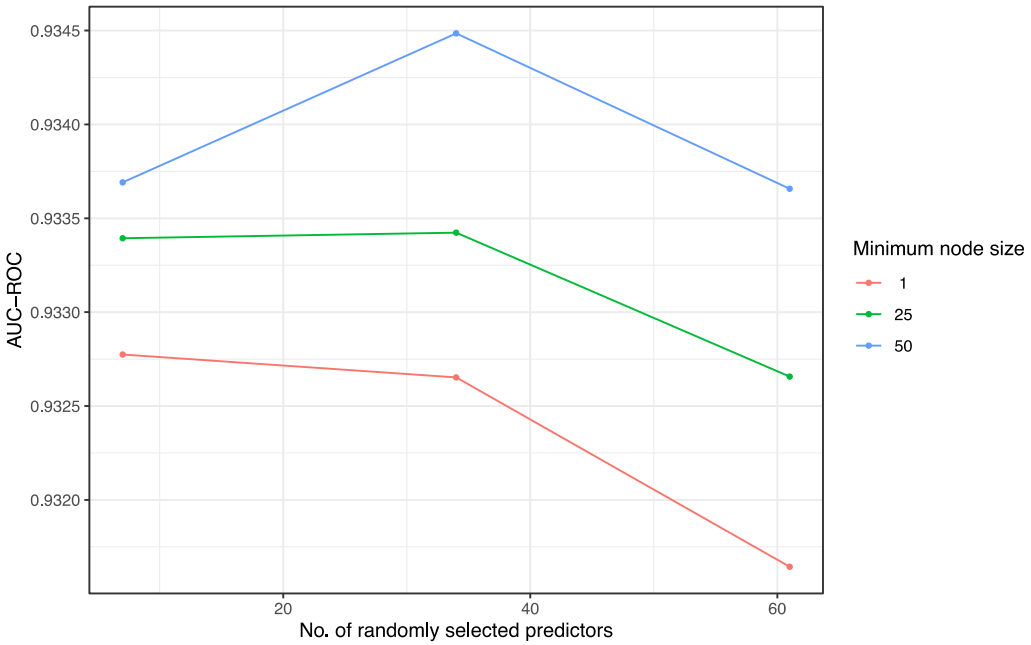

Figure 17. The area under the receiver operating characteristic curve (AUC-ROC) scores relative to the hyperparameters that were tuned as part of the extremely randomized trees model. These hyperparameters consist of the number of predictors that are randomly selected to be available at each node split (i.e., 'mtry') and the minimum number of observations that are required to form a leaf node of the tree.

Predictions from the landslide susceptibility model assign a probability value to each pixel, and this probability value reflects how similar the conditions are relative to those occurring at locations with active/historical slope failures. When these probabilities are used to classify the terrain into binary nonsusceptible/susceptible classes using a 0.5 cutoff threshold, the model yields moderately high performances (Figure 18a) based on the ability to predict holdout data during the spatial block cross-validation, with an overall accuracy of 0.84 and with a higher performance of predicting nonsusceptible areas (precision = 0.93), relative to predicting susceptible areas (recall = 0.73). The AUC-ROC score for the model also shows an overall high-level performance, 0.94 (Figure 18b), where 1 is a perfect ability to predict each class, and 0.5 is equivalent to a random guess.

The landslide susceptibility model of the Alberta Plains and shield regions, version 2, uses six categories of susceptibility and the accuracy of predicting landslides (based on precision and recall) within each category is shown in Figure 19. For example, using a very conservative threshold in the ‘very low’ category will result in a recall score of 0.996 (almost all historical landslide locations are detected) but this will also include a larger number of false positives (precision = 0.629). A threshold in the ‘medium’ category will result in a recall score of 0.82 and has a reasonably high precision of 0.9. Finally, using only the ‘high’ or ‘very high’ categories will lead to many potential landslides being missed (recall = ~0.3) but these categories could be used to identify areas that are extremely susceptible to developing new failures, such as on the outer banks of large rivers.

7 Susceptibility Map Prediction

The landslide susceptibility map (AGS Map 627 [Pawley et al., 2022a]; Figure 20) was produced by applying the susceptibility model to the stack of raster-based predictors. The predicted probabilities can be displayed as their raw values or binned into the six (very low to very high) categories. Digital data for

the susceptibility values are published as a raster dataset in AGS Digital Data 2022-0006 (Pawley et al. 2022b). The remaining area with no-data values is the area that is outside of the predicted landslide-prone area. Within the landslide-prone area, the probabilities of the pixels represent the potential for developing new failures or landslide reactivation.

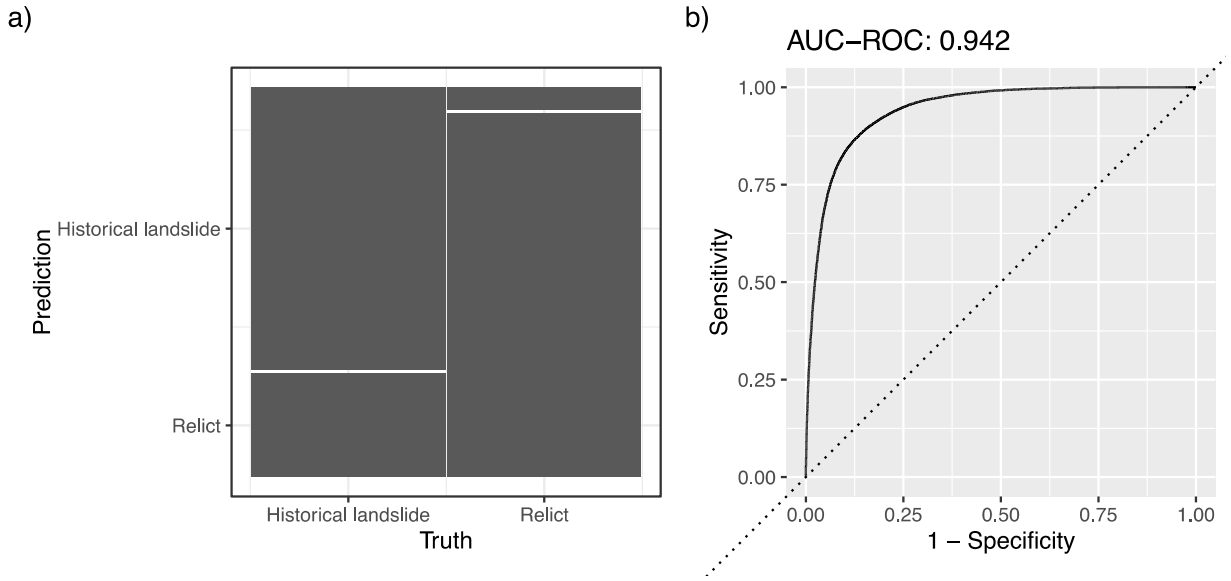

Figure 18. (a) Mosaic plot of the confusion matrix for the landslide susceptibility model, based on a 0.5 cutoff threshold, and (b) receiver-operating characteristic curve (ROC) and area under the curve (AUC-ROC) for the landslide susceptibility model.

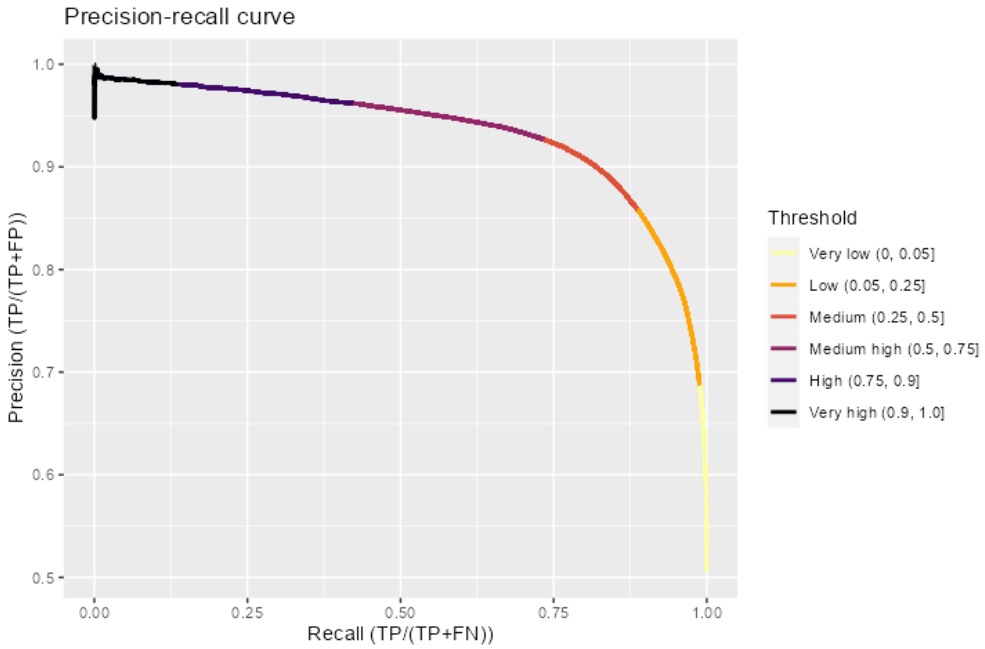

Figure 19. Precision and recall scores based on manually defined cutoff thresholds between the landslide and background classes. These cutoff thresholds represent the divisions that are used to categorize the susceptibility values for the map. Abbreviations: FN, total number of false negatives; FP, total number of false positives; TP, total number of true positives.

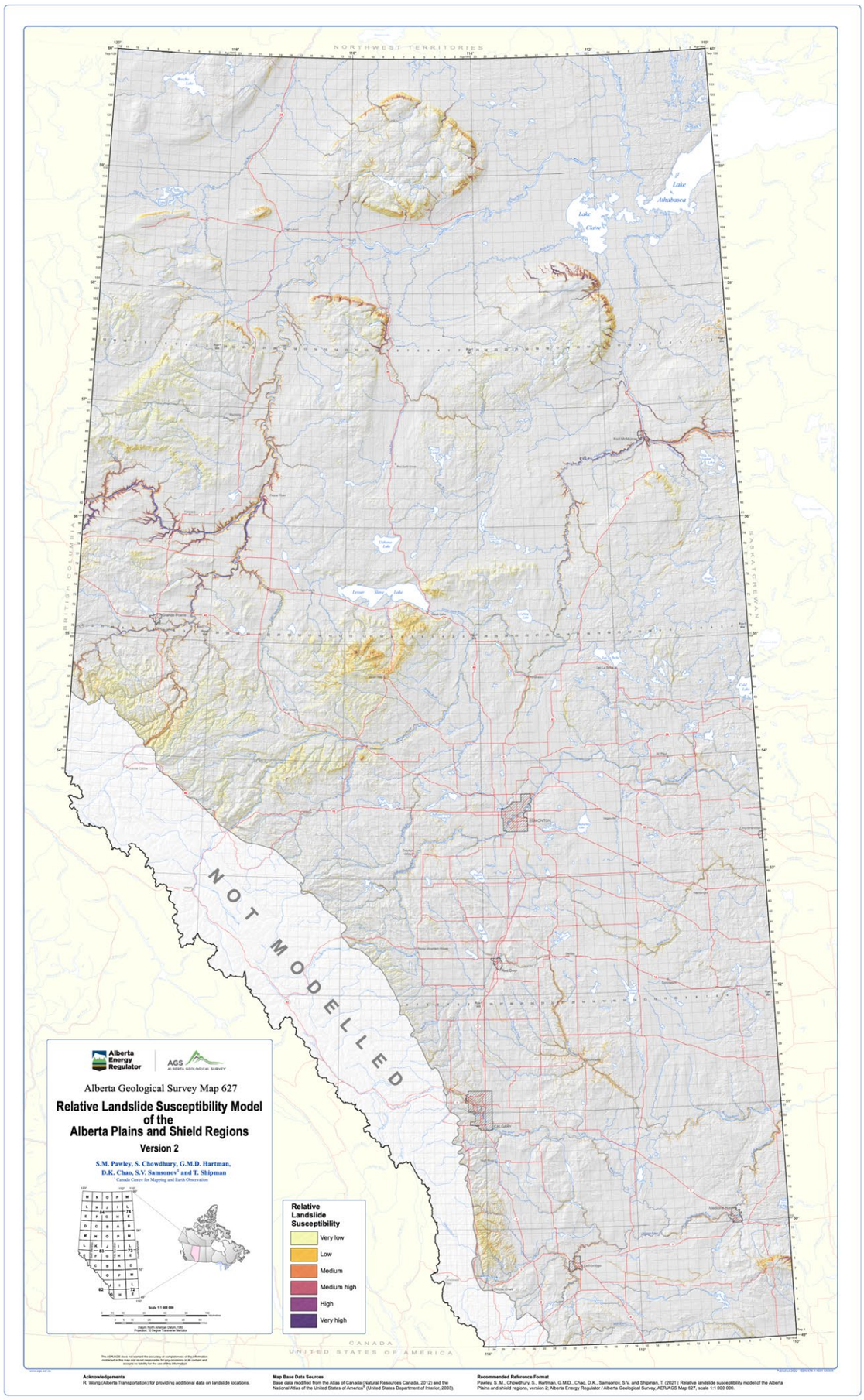

Figure 20. Map produced from the predicted landslide susceptibility model of the Alberta Plains and shield regions (version 2; Pawley et al., 2022a).

The susceptibility predictions show strong relationships with erosion-driven landslides, as highly susceptible areas are mostly restricted to the outer banks of major rivers in southern and central Alberta. However, in northern Alberta, most major river valleys are continuously flanked by much broader and near contiguous zones of high susceptibility. Other regions in southern Alberta where steeply sloping terrain results from high erosion rates, such as in a badlands-type setting, have low susceptibility ratings because landslides are relatively rare under these circumstances. Other areas of low to medium susceptibility include uplands in central and northern Alberta, as well as around the northern flank of the Cypress Hills. In these regions, the highest susceptibility estimates are associated with terrain that is dissected by networks of rivers and gullies and is being actively eroded. Medium susceptibility estimates are also associated with broader areas containing colluvial deposits, where small numbers of failures are also reported within the landslide susceptibility inventory.

7.1 Changes between Version 1 and Version 2

Comparison of the version 2 landslide susceptibility predictions with those of version 1 (Figure 21) show that the overall footprint of predicted landslide terrain is similar between the two models, albeit version 2 is more refined because higher resolution LiDAR topographic information was used compared to the lower resolution SRTM data used for version 1. However, the susceptibility ratings differ between the two products because version 2 is based on the spatial distribution of historically active landslides (those that have occurred during the past 50–100 years approximately), whereas version 1 is based on the geomorphological record of past landslides, which includes many landslides that are potentially relict and/or of early to middle Holocene age.

Consequently, the version 1 predictions consider large swathes of landslide terrain that show little evidence of recent movement to be as highly susceptible as areas with highly active landslides, such as in the Peace River region. In contrast, the version 2 predictions still retain the overall landslide footprint in the model predictions, but regions with many reported slope failures are rated to be much more susceptible than other areas. The version 2 predictions are therefore much more suited to identifying regions where future landslides are most likely to occur, while also preserving the total extent.

The version 2 landslide susceptibility predictions were also produced at a substantially higher resolution (30 m horizontal resolution) than version 1 (90 m). This means that local areas of susceptibility, for example, along the outer banks of many river systems (Figure 22), can also be accurately distinguished in the predictions in comparison to other steeply sloping terrain, such as gullied/badlands-type topography, that overall is not landslide prone.

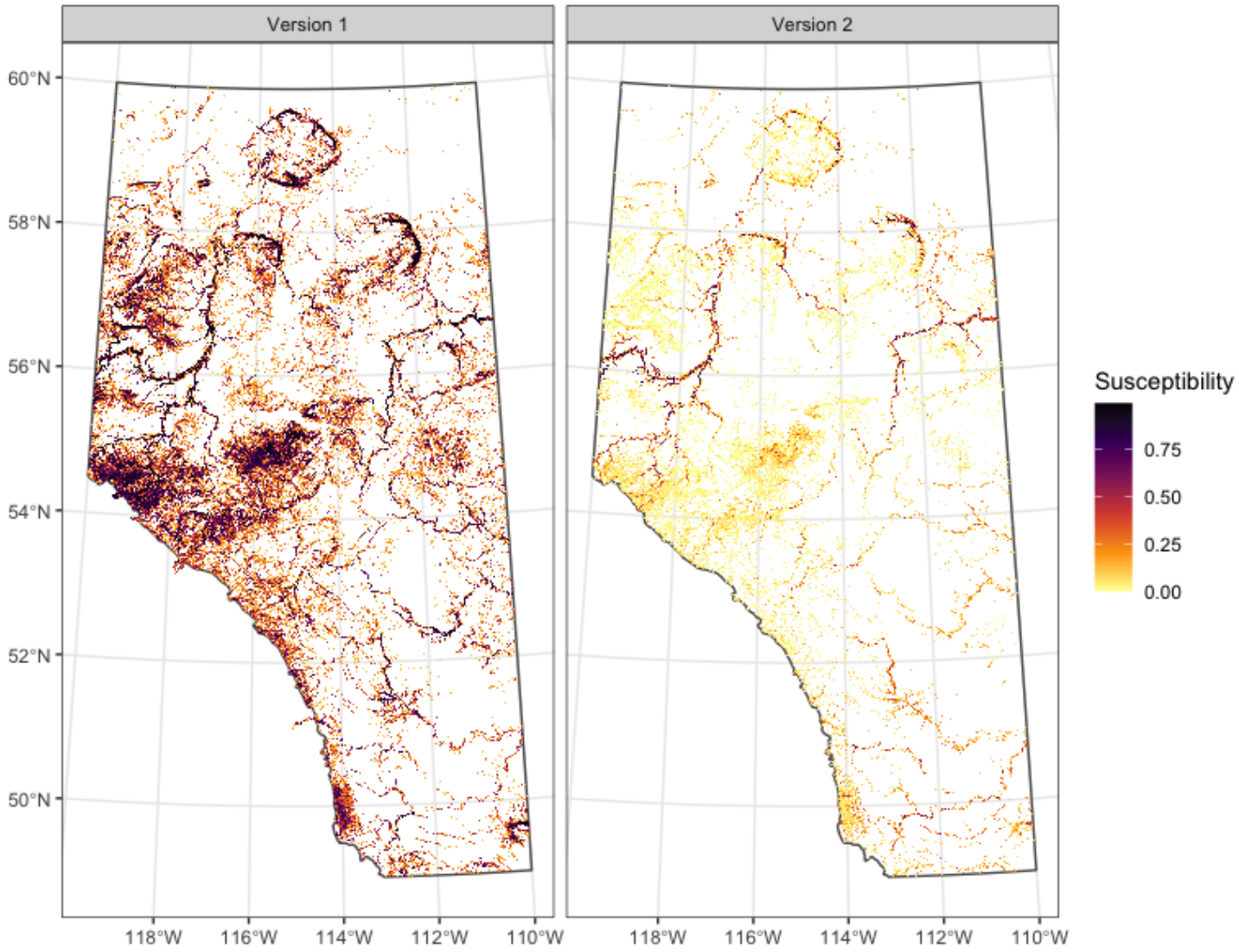

Figure 21. Comparison of the landslide susceptibility predictions between versions 1 and 2 of the landslide susceptibility model of the Alberta Plains and shield regions (Pawley et al., 2016, 2022b). Note that both maps display a reduced resolution version of the digital data.

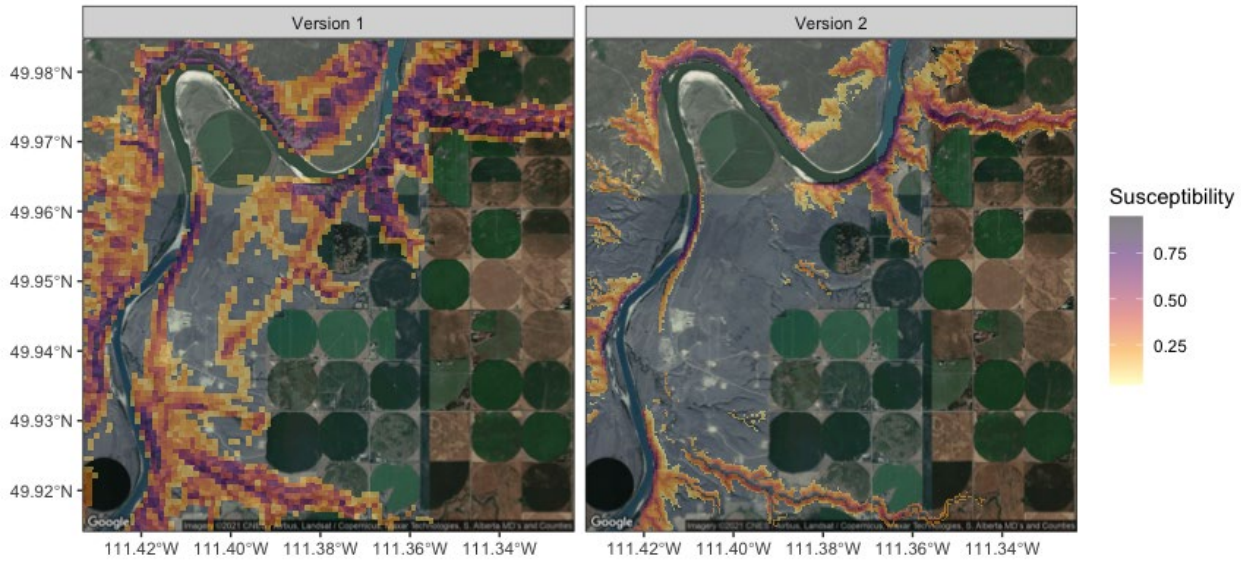

Figure 22. Level of detail differences between versions 1 and 2 of the landslide susceptibility model of the Alberta Plains and shield regions (Pawley et al., 2016, 2022b). Imagery © CNES/Airbus, Landsat/Copernicus, Maxar Technologies, S. Alberta MD's and Counties.

8 Summary

This study developed a machine learning approach that updates the previously published landslide susceptibility model of the Alberta Plains and shield regions. The new version 2 model makes use of higher resolution topographic information from a digital elevation model (DEM), created from light detection and ranging (LiDAR) data, and incorporates a new landslide inventory consisting of landslide locations that have occurred over a historical time period (during the past 50–100 years approximately). These landslide locations were compiled from multiple data sources including mapping from high-resolution multitemporal satellite imagery and ground motion rates from interferometric synthetic aperture radar (InSAR) data. This information was used in a machine learning model to predict the spatial locations where future landslides are more likely to occur, while also refining the overall distribution of landslide terrain. Although these predictions provide realistic estimates as to where future landslides are more likely to occur, they do not provide any constraints as to when any new landslides may potentially develop. Furthermore, the machine learning model relies upon many regional-scale factors and, as such, cannot accurately account for localized to site-specific variations in susceptibility. Instead, it highlights areas where more detailed, site-specific evaluations may need to be undertaken to identify potential risks resulting from slope failures.

9 References

Atkinson, L.A., Pawley, S.M., Andriashek, L.D., Hartman, G.M.D., Utting, D.J. and Aktinson, N. (2020): Sediment thickness of Alberta, version 2; Alberta Energy Regulator / Alberta Geological Survey, AER/AGS Map 611, scale 1:1 000 000, URL <https://ags.aer.ca/data-maps-models/maps/map-611> [March 2022].

Atkinson, N., Utting, D.J. and Pawley, S.M. (2014): Landform signature of the Laurentide and Cordilleran Ice sheets across Alberta during the last glaciation; Canadian Journal of Earth Sciences, v. 51, p. 1067–1083, doi:10.1139/cjes-2014-0112

Böhner, J. and Selige. T. (2006): Spatial prediction of soil attributes using terrain analysis and climate regionalisation; *in* SAGA - Analyses and Modelling Applications, J. Böhner, K.R. McCloy and J. Strobl (ed.), Göttinger Geographische Abhandlungen, v. 115, p. 13–28.

Böhner, J., Selige, T. and Ringeler, A. (2006): Image segmentation using representativeness analysis and region growing; *in* SAGA - Analyses and Modelling Applications, J. Böhner, K.R. McCloy and J. Strobl (ed.), Göttinger Geographische Abhandlungen, v. 115, p. 29–38.

Castilla, G., Hird, J., Hall, R.J., Schieck, J. and McDermid, G.J. (2014): Completion and updating of a Landsat-based land cover polygon layer for Alberta, Canada; Canadian Journal of Remote Sensing, v. 40, p. 92–109, doi:10.1080/07038992.2014.933073

Chen, T. and Guestrin, C. (2016): XGboost: a scalable tree boosting system; *in* Proceedings of the 22nd ACM SIGKDD International Conference on Knowledge Discovery and Data Mining, p. 785–794, doi:10.1145/2939672.2939785

Conrad, O., Bechtel, B., Bock, M., Dietrich, H., Fischer, E., Gerlitz, L., Wehberg, J., Wichmann, V. and Böhner, J. (2015): System for automated geoscientific analyses (SAGA) v. 2.1.4; Geoscientific Model Development, v. 8, p. 1991–2007, doi:10.5194/gmd-8-1991-2015

Dewitte, O., Chung, C-J., Cornet, Y., Daoudi, M. and Demoulin, A. (2010): Combining spatial data in landslide reactivation susceptibility mapping: a likelihood ratio-based approach in W Belgium; Geomorphology, v. 122, p. 153–166, doi:10.1016/j.geomorph.2010.06.010

Fenton, M.M., Waters, E.J., Pawley, S.M., Atkinson, N., Utting, D.J. and Mckay, K. (2013): Surficial geology of Alberta; Alberta Energy Regulator, AER/AGS Map 601, scale 1:1 000 000, URL <https://ags.aer.ca/publication/map-601> [March 2022].

Gallant, J.C. and Dowling, T.I. (2003): A multiresolution index of valley bottom flatness for mapping depositional areas; Water Resources Research, v. 39, no. 12, art. 1347, doi:10.1029/2002WR001426

Iwahashi, J. and Pike, R.J. (2007): Automated classifications of topography from DEMs by an unsupervised nested-means algorithm and a three-part geometric signature; Geomorphology, v. 86, p. 409–440, doi:10.1016/j.geomorph.2006.09.012

Miller, B.G.N. (2000): Two landslides and their dams, Peace River Lowlands, Alberta; Ph.D. thesis, University of Alberta.

Miller, B.G.N. and Cruden, D.M. (2002): The Eureka River landslide and dam, Peace River Lowlands, Alberta; Canadian Geotechnical Journal, v. 39, p. 863–878.

Morgan, A.J., Paulen, R.C., Slattery, S.R. and Froese, C.R. (2012): Geological setting for large landslides at the Town of Peace River, Alberta (NTS 84C); Energy Resources Conservation Board, ERCB/AGS OFR 2012-04, 33 p., URL <https://ags.aer.ca/publication/ofr-2012-04> [March 2022].

Olaya, V. (2009): Basic land-surface parameters; Developments in Soil Science, v. 33, p. 141–169.

Parise, M. (2001): Landslide mapping techniques and their use in the assessment of the landslide hazard; Physics and Chemistry of the Earth, Part C: Solar, Terrestrial & Planetary Science, v. 26, p. 697–703, doi:10.1016/S1464-1917(01)00069-1

Pawley, S.M. (2021): Rsagacmd: linking R with the open-source 'SAGA-GIS' software; R package version 0.1.1., URL <https://CRAN.R-project.org/package=Rsagacmd> [March 2022].

Pawley, S.M., Hartman, G.M.D. and Chao, D.K. (2016): Relative landslide susceptibility model of the Alberta Plains and shield regions; Alberta Energy Regulator, AER/AGS Map 605, scale 1:1 000 000, URL <https://ags.aer.ca/publication/map-605> [March 2022].

Pawley, S.M., Chowdhury, S., Hartman, G.M.D., Chao, D.K., Samsonov, S.K. and Shipman, T.C. (2022a): Relative landslide susceptibility model of Alberta Plains and shield regions, version 2; Alberta Energy Regulator / Alberta Geological Survey, AER/AGS Map 627, scale 1:1 000 000.

Pawley, S.M., Chowdhury, S., Hartman, G.M.D., Chao, D.K., Samsonov, S.K. and Shipman, T.C. (2022b): Relative landslide susceptibility model of the Alberta Plains and shield regions, version 2 (gridded data, GeoTIFF format); Alberta Energy Regulator / Alberta Geological Survey, AER/AGS DIG 2022-0006.

Pawley, S.M., Chowdhury, S., Hartman, G.M.D., Chao, D.K., Samsonov, S.K. and Shipman, T.C. (2022c): Relative landslide susceptibility model of the Alberta Plains and shield regions, version 2 (tabular data); Alberta Energy Regulator / Alberta Geological Survey, AER/AGS DIG 2022-0007.

Porter, M., Van Hove, J., Barlow, P., Froese, C. and Bunce, C. (2019): The estimated economic impacts of Prairie landslides in western Canada; *in* Proceedings of the 72nd Canadian Geotechnical Conference, September 29–October 2, 2019, St. John's, Newfoundland and Labrador, v. 29, 8 p.

Prior, G.J., Hathway, B., Glombick, P.M., Pana, D.I., Banks, C.J., Hay, D.C., Schneider, C.L., Grobe, M., Elgr, R. and Weiss, J.A. (2013): Bedrock geology of Alberta; Alberta Energy Regulator, AER/AGS Map 600, scale 1:1 000 000, URL <https://ags.aer.ca/publication/map-600> [March 2022].

R Core Team (2020): R: a language and environment for statistical computing; R Foundation for Statistical Computing, Vienna, Austria.

Reichenbach, P., Rossi, M., Malamud, B.D., Mihir, M. and Guzzetti, F. (2018): A review of statistically-based landslide susceptibility models; Earth-Science Reviews, v. 180, p. 60–91, doi:10.1016/j.earscirev.2018.03.001

Riley, S.J., DeGloria, S.D. and Elliot, R. (1999): Index that quantifies topographic heterogeneity; Intermountain Journal of Sciences, v. 5, p. 23–27.

Ruban, A.F. (1983): A report on slope instability along the Oldman River and tributaries in the vicinity of Lethbridge, Alberta; M.Sc. thesis, University of Alberta, 138 p.

Samsonov, S.V. and d'Oreye, N. (2017): Multidimensional small baseline subset (MSBAS) for two-dimensional deformation analysis: case study Mexico City; Canadian Journal of Remote Sensing, v. 43, p. 318–329, doi:10.1080/07038992.2017.1344926

Sappington, J.M., Longshore, K.M. and Thompson, D.B. (2007): Quantifying landscape ruggedness for animal habitat analysis: a case study using bighorn sheep in the Mojave Desert; Journal of Wildlife Management, v. 71, p. 1419–1426, doi:10.2193/2005-723

Thomson, S. and Morgenstern, N.R. (1977): Factors affecting distribution of landslides along rivers in southern Alberta; Canadian Geotechnical Journal, v. 14, p. 508–523.

Wang, T., Hamann, A., Spittlehouse, D.L. and Murdock, T.Q. (2012): ClimateWNA high-resolution spatial climate data for western North America; Journal of Applied Meteorology and Climatology, v. 51, p. 16–29.

Wood, J. (1996): The geomorphological characterisation of digital elevation models; Ph.D. thesis, University of Leicester.

Yokoyama, R., Shlrasawa, M. and Pike, R.J. (2002): Visualizing topography by openness: a new application of image processing to digital elevation models; Photogrammetric Engineering and Remote Sensing, v. 68, p. 257–265.